Geological Magazine

www.cambridge.org/geo

Original Article

Cite this article: Zhang X, Chai F, Chen C, Quan H, and Gong X. (2020) Geochronology, geochemistry and tectonic implications of late Carboniferous Daheyan intrusions from the Bogda Mountains, eastern Tianshan. *Geological Magazine* **157**: 289–306. doi: 10.1017/S001675681900075X

Received: 8 January 2019
Revised: 20 May 2019
Accepted: 26 May 2019
First published online: 29 July 2019

Keywords:
U–Pb zircon age; geochemistry; Hf isotope; Bogda Mountains; tectonic setting.

Author for correspondence: Xiaoping Gong, Email: 504642842@qq.com

CAMBRIDGE UNIVERSITY PRESS

Geochronology, geochemistry and tectonic implications of late Carboniferous Daheyan intrusions from the Bogda Mountains, eastern Tianshan

Xuebing Zhang[1], Fengmei Chai[1], Chuan Chen[1], Hongyan Quan[2] and Xiaoping Gong[1]

[1]College of Geology and Mining Engineering, Xinjiang University, Urumqi 830047, China and [2]School of Biological, Earth and Environmental Sciences, University of New South Wales, Kensington, New South Wales 2052, Australia

Abstract

The Daheyan region, situated in the SW of the Bogda Mountains in eastern Tianshan, is important for understanding the accretionary history of the Central Asian Orogenic Belt. We investigated Carboniferous intrusions from the Daheyan area, SW Bogda Mountains, obtaining new zircon U–Pb ages, whole-rock geochemical data and Hf isotope data for these intrusions. Zircon U–Pb dating indicates that syenogranite, diorite, granodiorite and monzonite of the Daheyan intrusions were all formed during late Carboniferous (311–303 Ma) magmatism. The syenogranite has geochemical characteristics of A-type granites that were mainly sourced from melting of juvenile crust. In comparison, the low-Mg-number diorite intrusion, with tholeiite and metaluminous features, was derived from young crust and mixed some mantle materials. The granodiorite and monzonite are both I-type granites, and are both sourced from the melting of juvenile crust. Based on a comprehensive analysis of previous geochronological, geochemical and isotopic data of magmatic and sedimentary rocks in the Bogda–Harlik belt, we consider that late Carboniferous intrusive rocks of the Bogda Mountains formed in an intra-arc extension related to a continent-based arc setting.

1. Introduction

The Central Asian Orogenic Belt (CAOB) is one of the largest and longest-lived accretionary orogenic collages in the world, with considerable Neoproterozoic and Phanerozoic crustal growth (Jahn *et al.* 2000; Xiao *et al.* 2004, 2013, 2017; Yakubchuk, 2017). It experienced a long and complex geological history, for example, the successive amalgamation and multiple collisions of accretionary wedges, island arcs, microcontinents and oceanic seamounts (Xiao *et al.* 2013; Xie *et al.* 2016*a*, *b*, *c*; Wali *et al.* 2018).

In the Bogda Mountains, located in the northern segment of the eastern Tianshan, SW CAOB, Carboniferous–Permian volcanic rocks and coeval intrusive rocks are well developed, including Daheyan intrusions. There is also an important ore province in northeastern Tianshan, and many late Carboniferous Cu polymetallic deposits, for example, the deposits of Tonggou, Miao'ergou, Xingshugou and Weicaogou, have been discovered and exploited. However, the late Palaeozoic tectonic setting of the Bogda Mountains is still the subject of strong debate concerning island-arc-, rifting- and mantle-plume-related large igneous provinces, post-collisional extension and intra-arc extension setting (Gu *et al.* 2000, 2001; Shu *et al.* 2005, 2011; Xie *et al.* 2016*a*, *b*, *c*; Wali *et al.* 2018). Numerous late Carboniferous intermediate-felsic intrusions have been found in the Daheyan area of the Bogda Mountains during regional geological surveying in recent years. These intrusions contain plenty of geological information about the tectonic evolutionary history of eastern Tianshan and can greatly contribute to our understanding of the suture zone. It is therefore a key area for understanding the late Palaeozoic geodynamic setting of mineralization and tectonic evolution of eastern Tianshan.

The Daheyan area is located in the southwestern Bogda Mountains, eastern Tianshan and Daheyan intrusions crop out to the north of the town of Daheyan. This study presents detailed zircon U–Pb, whole-rock geochemical and Hf isotope analyses for the intrusions. We discuss the tectonic setting and geodynamic evolution of eastern Tianshan during *c*. 311–303 Ma. We also address the tectonic setting of Cu polymetallic mineralization in the Bogda Mountains.

2. Regional tectonic setting

The E–W-striking Chinese Tianshan Belt is a major tectonic unit in the southernmost part of the CAOB (Fig. 1a; Allen *et al.* 1993). The eastern Tianshan is the east part of the Chinese Tianshan

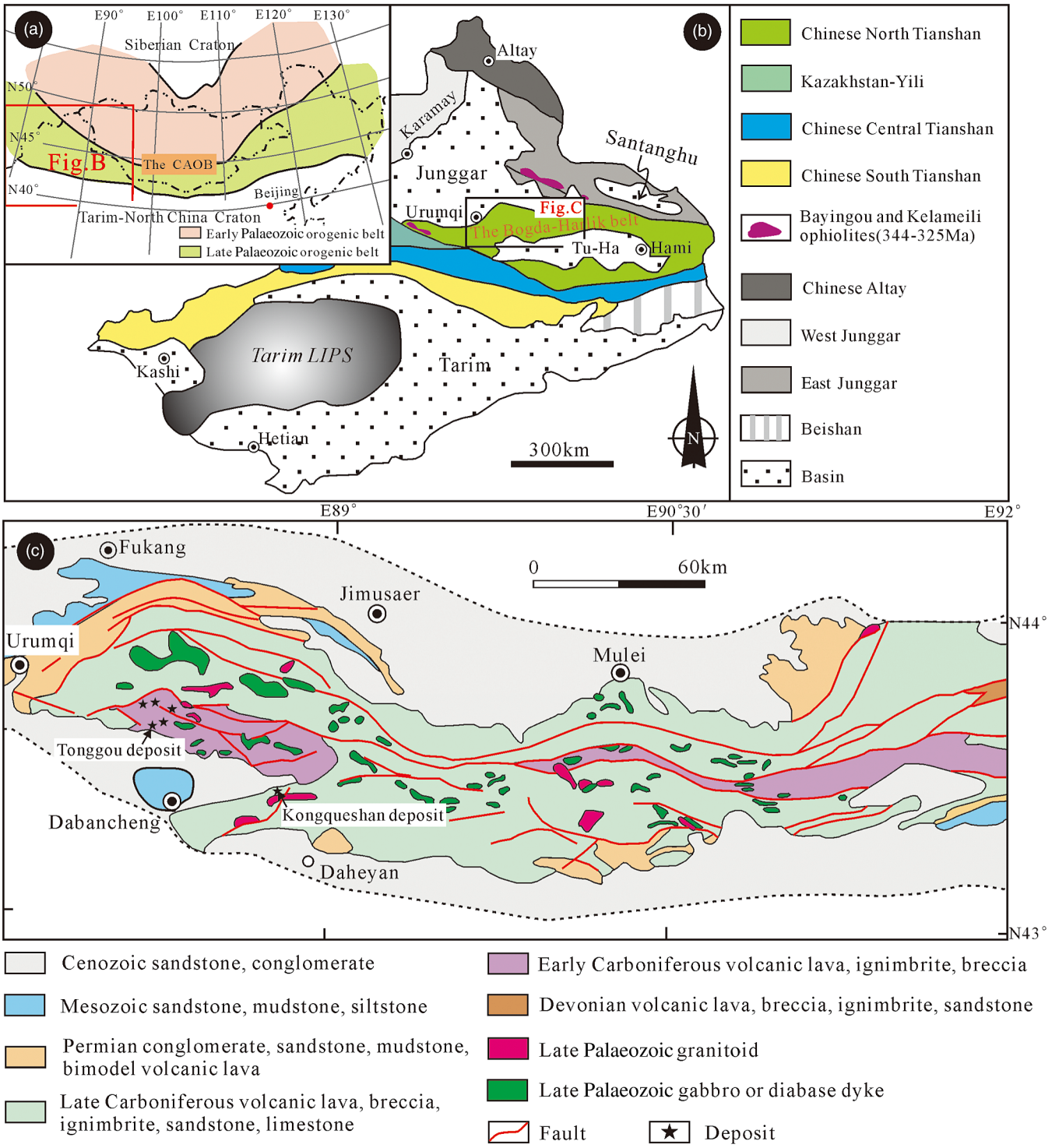

Fig. 1. (Colour online) (a) Schematic geological map of the Central Asian Orogenic Belt (CAOB); (b) simplified tectonic sketch map of most of Xinjiang Province, NW China (modified after Pirajno *et al.* 2008; Wang *et al.* 2011; Xiao *et al.* 2013); and (c) geological map of the Bogda Orogenic Belt at the north margin of the Chinese North Tianshan (modified after Chen *et al.* 2010; Zhao *et al.* 2014).

Belt, and is bounded by the Junggar Block to the north and the Precambrian Tarim Block to the south (Fig. 1b; Zhang *et al.* 2003; Han *et al.* 2010). This belt witnessed the opening and closure of the Palaeo-Asian ocean during Palaeozoic–Triassic time (Allen *et al.* 1995; Carroll *et al.* 1995; Wu *et al.* 2007; Xu *et al.* 2012), and experienced multiple accretion, collision and mineralization events (Xiao *et al.* 2004, 2013). This area is subdivided into four tectonic units (from north to south): (1) the Bogda-Harlik Orogenic Belt, which is bounded by the Junggar basin in the north and the Turpan-Hami basin in the south; (2) the Dananhu-Tousuquan Zone, which is situated north of the Kangguer Fault; (3) the Kanggur-Yamansu-Heiyingshan Zone, which is between the Kangguer and Aqikuduke faults; and (4) the Central Tianshan Massif, which lies between the Aqikuduke-Shaquanzi Fault in

https://doi.org/10.1017/S001675681900075X Published online by Cambridge University Press

the north and the Hongliuhe-Xingxingxia and Kawabulak faults in the south (Fig. 1b; Qin *et al.* 2011; Su *et al.* 2012; Wu *et al.* 2016).

The Bogda Mountains extends over 360 km from east to west along the northern margin of eastern Tianshan. The oldest formation in the Bogda Mountains is Devonian strata, which are dominated by marine and terrigenous sediments, tuffaceous sandstone and volcanic rocks. Carboniferous strata are widely exposed in the Bogda Mountains and are in fault contact with the Devonian rocks (Fig. 1c). The Carboniferous strata are divided into three formations, namely, the Lower Carboniferous Qijiaojing Formation and the Upper Carboniferous Liushugou and Qijiagou formations (BGMRXUAR, 1993; Gu *et al.* 2001; Xia *et al.* 2004; Liang *et al.* 2011). The Lower and Upper Carboniferous formations are separated by regional faults (Fig. 1c). The Lower Carboniferous Formation mainly consists of marine volcanic ignimbrites, tuffaceous sandstone and bimodal volcanic lavas, while the Upper Carboniferous Formation is dominated by marine (pillow) basaltic lava and felsic ignimbrites, with minor sandstone and siltstone. Permian strata are unconformably overlying the Carboniferous rocks. In this region, the Permian strata are mainly composed of terrestrial conglomerate, sandstone and siliceous mudstone intercalated with bimodal volcanic lavas. Jurassic clastic sediments occur in the SE of the study area and unconformably overlie the Permian strata (Fig. 1c; Carroll *et al.* 1990; BGMRXUAR, 1993). Many approximately E–W-trending folds and faults are well developed in the Bogda Mountains. These folds mainly include the Miao'ergou anticline and Tonggou syncline, and a series of secondary E–W-trending faults are developed in the flanks of the folds (BGMRXUAR, 1993).

Late Palaeozoic intrusions crop out extensively in the Bogda Mountains (Fig. 1c), such as the Daheyan intrusion which is situated in the SW part of the Bogda Mountains. Zircon U–Pb ages indicate that intrusions in the Bogda Mountains are mostly of late Carboniferous (Sun *et al.* 2005; Han *et al.* 2010; Li *et al.* 2013; Si *et al.* 2014; Wang *et al.* 2015; Lei *et al.* 2016*a*) and early Permian (Gu *et al.* 2000; Yuan *et al.* 2010) in age. Late Carboniferous intrusive rocks consist of gabbro, diorite, granodiorite and granite. Early Permian intrusive rocks include diorite, monzogranite and granite. The Bogda Mountains hosts several Cu polymetallic deposits, for example, the Tonggou, Xingshugou, Miao'ergou and Weicaogou deposits. Re–Os isotopic analyses yield a chalcopyrite mineralization age of 303 ± 12 Ma (unpublished data), which indicates that the Tonggou deposit formed during late Carboniferous time. The Tonggou deposit shows a transition from a high-sulphidation epithermal to porphyry system; the Cu polymetallic mineralization may be associated with late Carboniferous magmatism.

3. Sample description and analytical methods

3.a. Sample description

Daheyan intrusions can be divided into Upper Daheyan and Lower Daheyan intrusions (Fig. 2). The Upper Daheyan intrusion lies 30 km east of Dabancheng, and mainly consists of syenogranite and diorite (Fig. 3). The Lower Daheyan intrusion lies 22 km east of Dabancheng, and mainly consists of granodiorite and monzonite (Fig. 3). In this study, we collected intrusive rocks from Daheyan intrusions, described in detail in the following.

Syenogranite was collected from an intrusion in the north of Daheyan (Fig. 2). The syenogranite is flesh red in colour and displays a subhedral and allotriomorphic texture in the mass, shows a graphic texture on the local scale and possesses a massive structure (Fig. 3a). It consists of quartz (20%), plagioclase (25%), alkali-feldspar (50%, including orthoclase and perthite), clinopyroxene (3%) (Fig. 3b) and minor accessory minerals (2%) that include apatite and zoisite.

Diorite was collected from an intrusion in the north of Daheyan (Fig. 2). The diorite is light red in colour, displays a subhedral and allotriomorphic texture, possesses a massive structure (Fig. 3c), and consists of plagioclase (76%), hornblende (22%), quartz (1%) and biotite (5%) (Fig. 3d).

Granodiorite was collected from an intrusion in the west of Daheyan (Fig. 2). The granodiorite is grey white, and commonly has a subhedral and allotriomorphic texture, and shows a massive structure (Fig. 3e). It consists of quartz (10%), plagioclase (77%), alkali-feldspar (6%, including orthoclase and perthite), chlorite (4%) and biotite (2%) (Fig. 3f).

Monzonite was collected from an intrusion in the west of Daheyan (Fig. 2). The monzonite is grey black, and commonly has a subhedral and allotriomorphic texture, and shows a massive structure (Fig. 3g). It consists of alkali-feldspar (53%, including orthoclase and perthite), quartz (10%), plagioclase (32%), hornblende (8%) and quartz (4%) (Fig. 3h).

3.b. Analytical methods

3.b.1. Zircon U–Pb dating

Zircon U–Pb ages were determined for samples from the Daheyan area (Fig. 2). Four samples were crushed, and zircon grains and cathodoluminescence (CL) images were generated at the Faith Geological Service Company, Langfang, Hebei province, China. U–Pb–Hf isotopic analyses of the zircons were performed at the Yanduzhongshi Geological Analysis Laboratories Ltd, Beijing. Zircon grains were mounted on epoxy blocks and polished to expose grain centres. CL images are shown in Figure 4. U–Pb dating and Hf isotopic analyses of zircons were obtained using an Agilent 7500a inductively coupled plasma (ICP) mass spectrometer (MS) and GeoLas 2005 laser ablation system. $^{206}Pb/^{238}U$ ratios were calculated by ICPMSDataCal (Liu *et al.* 2008, 2010), while the concordia age diagram and probability density plots of detrital zircon were obtained with Isoplot 3.0 (Ludwig, 2003).

3.b.2. Major and trace elements

Twelve samples of major, trace and rare earth elements were measured and analysed at ALS Minerals-ALS Chemex, Guangzhou. The samples were crushed in a steel jaw crusher and then powdered to 200 mesh in an agate mill. Major-element compositions were analysed using ME-XRF06 X. Trace and rare earth element compositions were analysed using ME-MS81 and ME-MS82.

4. Results

4.a. Zircon U–Pb dating

Syenogranite zircons exhibit oscillatory or planar zoning under CL, as is typical of magmatic zircons (Fig. 4a). The results of U–Pb dating for 30 zircons, collected from the syenogranite (sample D01) in the Daheyan area, are listed in Table 1. Th/U ratios range from 0.34 to 0.60, indicating that the origin of the zircons is magmatic (Hoskin & Black, 2000). Analysis reveals that 26 of the samples plot near the concordia curve (Fig. 4a, b). $^{206}Pb/^{238}U$ ages range from 304 to 313 Ma, with a mean of 307.7 ± 1.2 Ma (MSWD = 0.74), which represents the crystallization age of the syenogranite.

https://doi.org/10.1017/S001675681900075X Published online by Cambridge University Press

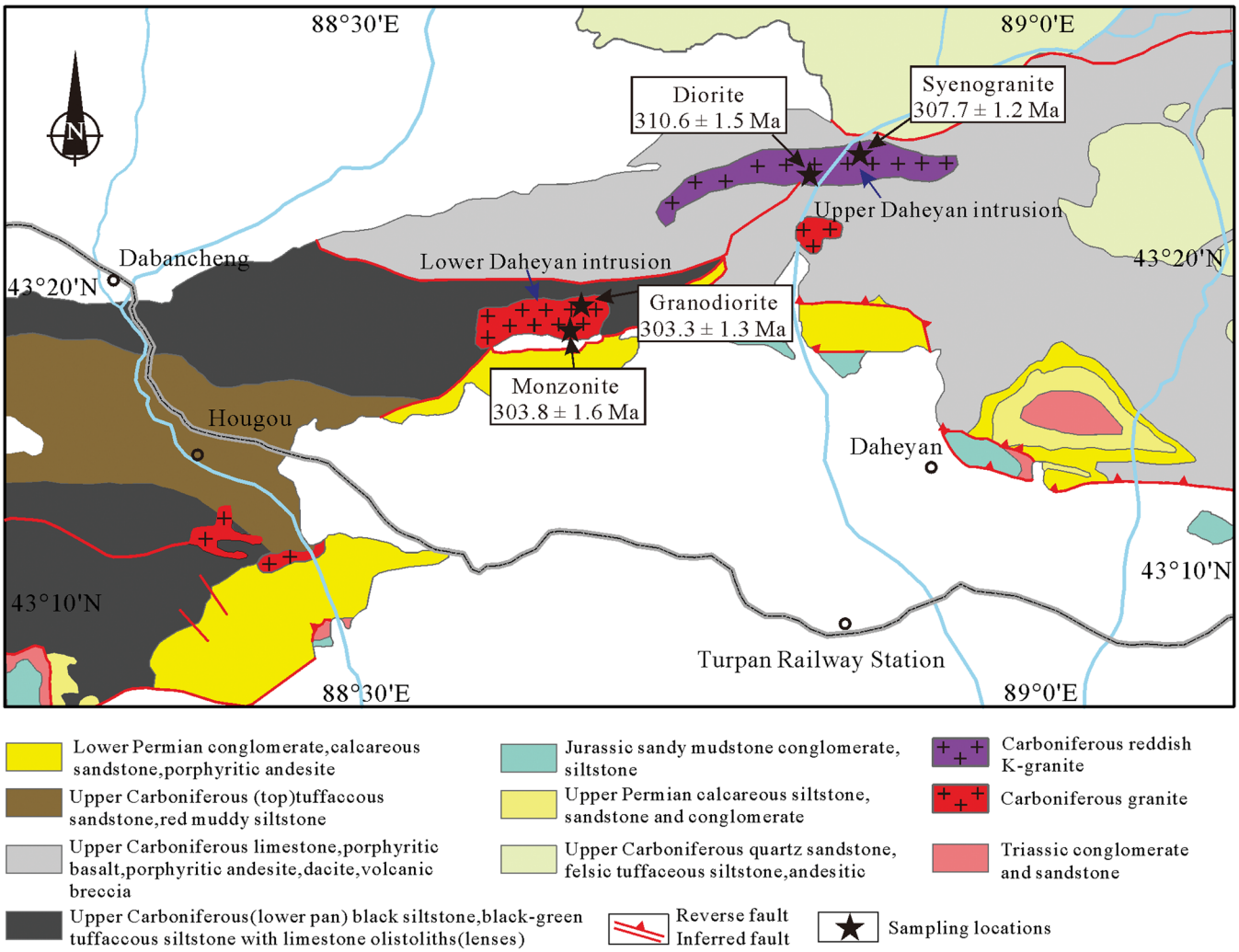

Fig. 2. (Colour online) Geological map of the Daheyan area, southern Bogda Range (compiled from the 1:200,000 map by XBGMR 1988).

In addition, one of the samples has a $^{206}Pb/^{238}U$ age of 339 Ma, which represents the crystallization age of zircons captured or entrained from the wall rock during magma ascent. The other three measured points deviate from the concordia curve.

Diorite zircons exhibit oscillatory or planar zoning under CL, as is typical of magmatic zircons (Fig. 4c). The results of U–Pb dating for 24 zircons, collected from the diorite (sample D02) in the Daheyan area, are listed in Table 1. Th/U ratios range from 0.44 to 1.11, indicating that the origin of the zircons is magmatic (Hoskin & Black, 2000). Analysis reveals that nine of the samples plot near the concordia curve (Fig. 4c, d). $^{206}Pb/^{238}U$ ages range from 308 to 312 Ma, with a mean of 310.6 ± 1.5 Ma (MSWD = 0.22), which represents the crystallization age of the diorite. In addition, 11 of the samples have $^{206}Pb/^{238}U$ ages varying from 324 to 327 Ma, which represents the crystallization age of zircons captured or entrained from the wall rock during magma ascent. The other four measured points deviate from the concordia curve.

Granodiorite zircons exhibit oscillatory or planar zoning under CL, as is typical of magmatic zircons (Fig. 4e). The results of U–Pb dating for 30 zircons collected from the granodiorite (sample D03) in the Daheyan area are listed in Table 1. Th/U ratios range from 0.23 to 0.75, indicating a magmatic origin for the zircons (Hoskin & Black, 2000). Analysis reveals that 20 of the samples plot near the concordia curve (Fig. 4e, f). $^{206}Pb/^{238}U$ ages range from 301 to 305 Ma, with a mean of 303.3 ± 1.3 Ma (MSWD = 0.28), which represents the crystallization age of the granodiorite. In addition, six of the samples have $^{206}Pb/^{238}U$ ages that vary from 354 to 360 Ma, which represents the crystallization age of zircons captured or entrained from the wall rock during magma ascent. The other four measured points deviate from the concordia curve.

Monzonite zircons exhibit oscillatory or planar zoning under CL, as is typical of magmatic zircons (Fig. 4g). The results of U–Pb dating for 30 zircons collected from the monzonite (sample D03) in the Daheyan area are listed in Table 1. Th/U ratios range from 0.41 to 0.78, indicating a magmatic origin for the zircons (Hoskin & Black, 2000). Analysis reveals that 21 of the samples plot near the concordia curve (Fig. 4g, h). $^{206}Pb/^{238}U$ ages range from 302 to 307 Ma, with a mean of 303.8 ± 1.6 Ma (MSWD = 0.12), which represents the crystallization age of the monzonite. In addition, $^{206}Pb/^{238}U$ ages of some samples are 326, 327, 351 and 361 Ma, which represents the crystallization age of zircons captured or entrained from the wall rock during magma ascent. The other five measured points deviate from the concordia curve.

https://doi.org/10.1017/S001675681900075X Published online by Cambridge University Press

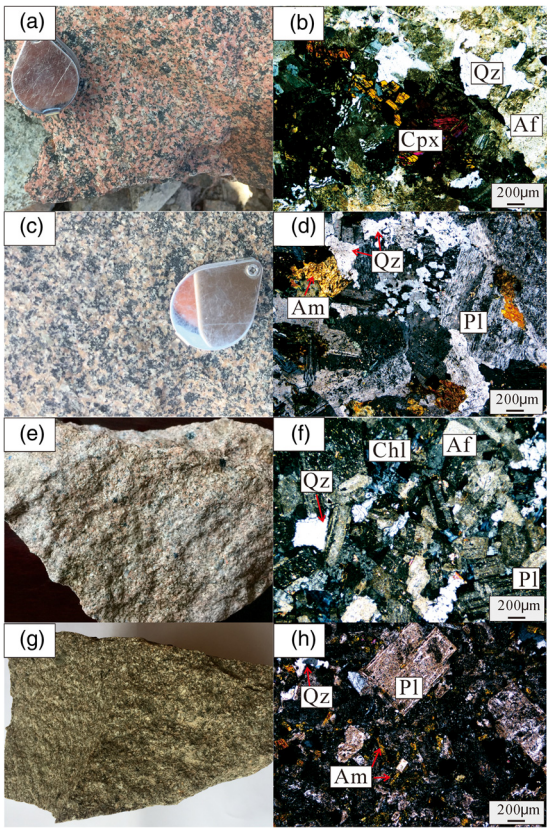

Fig. 3. (Colour online) Representative photographs of the magma rocks in hand specimen and thin-section in the Daheyan area. (a, b) syenogranite (D01); (c, d) diorite (D02); (e, f) granodiorite (D03); (g, h) monzonite (D04). Qtz – quartz; Or – orthoclase; Pl – plagioclase; Pth – perthite; Bt – biotite; Hbl – hornblende.

4.b. Major- and trace-element geochemistry

4.b.1. Major elements

Syenogranite shows SiO_2 enrichment (70.18–70.87 wt%), high $K_2O + Na_2O$ values (9.37–9.50 wt%), and Na_2O/K_2O = 0.88–1.11, with Al_2O_3 values of 13.34–13.43 wt%, total Fe_2O_3 values of 3.48–3.70 wt%, Mg number ($100Mg^{2+}/(Mg^{2+}+ TFe^{2+})$) of 5–19, and CaO values of 0.92–1.14 wt% (Table 2). All samples plot in the granite field on a SiO_2 versus K_2O+Na_2O diagram (Fig. 5a). The Rittmann index (σ) varies from 3.46 to 3.56 and, because of their high $K_2O + Na_2O$ values, all samples plot in the high-K calc-alkaline and shoshonite series range on a SiO_2 versus K_2O diagram (Fig. 5b). The A/CNK values range from 0.89 to 0.92 and plot in the metaluminous field on an A/CNK versus A/NK diagram (Fig. 5c).

Diorite has SiO_2 = 61.22–61.70 wt%, Al_2O_3 = 14.67–14.90 wt%, total Fe_2O_3 = 7.08–7.14 wt%, Mg no. = 33.7–33.8, CaO = 4.22 wt%, K_2O = 0.14–0.42 wt% and Na_2O = 7.55–7.76 wt% (Table 2). All samples plot in the monzonite field on a SiO_2 versus K_2O+Na_2O diagram (Fig. 5a). The Rittmann index (σ) varies from 3.92 to 4.00 and, because of their high Na_2O values, all samples plot in the tholeiite series range on a SiO_2 versus K_2O diagram (Fig. 5b). The A/CNK values approach 0.71 and plot in the metaluminous field on an A/CNK versus A/NK diagram (Fig. 5c).

Granodiorite shows high SiO_2 (68.14–68.67 wt%), K_2O (2.60–3.11 wt%) and Al_2O_3 (15.54–15.92 wt%). Na_2O values are 5.53–6.14 wt%, total Fe_2O_3 = 3.01–3.48 wt%, Mg no. = 29–33 and CaO = 1.12–1.60 wt% (Table 2). All samples plot in the quartz monzonite field on a SiO_2 versus $K_2O + Na_2O$ diagram (Fig. 5a). The Rittmann index (σ) varies from 2.99 to 3.29 and, because of their high Na_2O values, all samples plot in the high-K calc-alkaline and calc-alkaline series range on the SiO_2 versus K_2O diagram (Fig. 5b). A/CNK values range from 1.05 to 1.08 and plot in the peraluminous field on an A/CNK versus A/NK diagram (Fig. 5c).

Monzonite has and SiO_2 value of 61.50 wt%, K_2O of 2.86 wt%, Al_2O_3 of 14.68 wt%, Na_2O of 5.42 wt%, total Fe_2O_3 of 7.61 wt%, Mg no. 32 and CaO of 3.74 wt% (Table 2). Samples plot in the monzonite field on a SiO_2 versus K_2O+Na_2O diagram (Fig. 5a). The Rittmann index (σ) is 3.97 and, due to their high Na_2O, monzonite sample plots in the high-K calc-alkaline series range on a SiO_2 versus K_2O diagram (Fig. 5b). The A/CNK value is 0.78 and plots in the metaluminous field on an A/CNK versus A/NK diagram (Fig. 5c).

4.b.2. Trace elements

Syenogranite samples are slightly enriched in light rare earth elements (LREEs), depleted in heavy rare earth elements (HREEs) (LREE/HREE = 4.21–4.61; $(La/Yb)_N$ = 3.14–3.57) and show clear negative Eu anomalies (δEu = 0.34–0.36) on a chondrite-normalized rare earth element (REE) diagram (Fig. 6a; Table 2). A primitive-mantle-normalized trace-element diagram indicates that the rock is enriched in incompatible elements (e.g. Th, U, Zr and Hf) and some large-ion lithophile elements (LILE; e.g. K and Rb), and is depleted in high-field-strength elements (HFSE; e.g. Ta, Nb, Ti and Sr) (Fig. 6b).

Diorite samples are slightly enriched in LREEs, depleted in HREEs (LREE/HREE = 3.89–4.15; $(La/Yb)_N$ = 3.05–3.46), and show weak negative Eu anomalies (δEu = 0.63–0.67) on a chondrite-normalized REE diagram (Fig. 6c; Table 2). The primitive-mantle-normalized trace-element diagram indicates that the rock is enriched in incompatible elements (e.g. Th, U, Zr and Hf) and some LILEs (e.g. K, Rb, Sr and Ba), and depleted in HFSEs (e.g. Ta, Nb and Ti) (Fig. 6d).

Granodiorite samples are obviously enriched in LREEs and depleted in HREEs (LREE/HREE = 9.54–10.41; $(La/Yb)_N$ = 9.05–10.53). Granodiorite shows no negative Eu anomalies (δEu = 0.94–0.99) on the chondrite-normalized REE diagram (Fig. 6e; Table 2). The primitive-mantle-normalized trace-element diagram indicates that the rocks are enriched in incompatible elements (e.g. Th, U, Zr and Hf) and some LILEs (e.g. Rb), and depleted in HFSEs (e.g. Ta, Nb and Ti) (Fig. 6f).

Monzonite samples are slightly enriched in LREEs and depleted in HREEs (LREE/HREE = 9.54–10.41; $(La/Yb)_N$ = 9.05–10.53). Monzonite shows weak negative Eu anomalies (δEu = 0.65) on the chondrite-normalized REE diagram (Fig. 6g; Table 2). The primitive-mantle-normalized trace-element diagram indicates that the rock is enriched in incompatible elements (e.g. Th, U, Zr and Hf) and some LILEs (e.g. K and Rb), and depleted in HFSEs (e.g. Ta, Nb, Ti and Sr) (Fig. 6d).

4.c. Hf isotopes

In situ Hf isotopic compositions of zircon from the syenogranite, diorite, granodiorite and monzonite are listed in Table 3.

The 24 analyses of sample D01 from syenogranite display variable initial Hf isotopic compositions, with $^{176}Hf/^{177}Hf$ = 0.0009–0.0023, and $\epsilon_{Hf}(t)$ values of +11.2 to +14.4. The corresponding single-stage model ages (T_{DM1}) range from *c.* 367 Ma to *c.* 499 Ma and two-stage model ages (T_{DM2}) range from *c.* 400 Ma to *c.* 606 Ma.

https://doi.org/10.1017/S001675681900075X Published online by Cambridge University Press

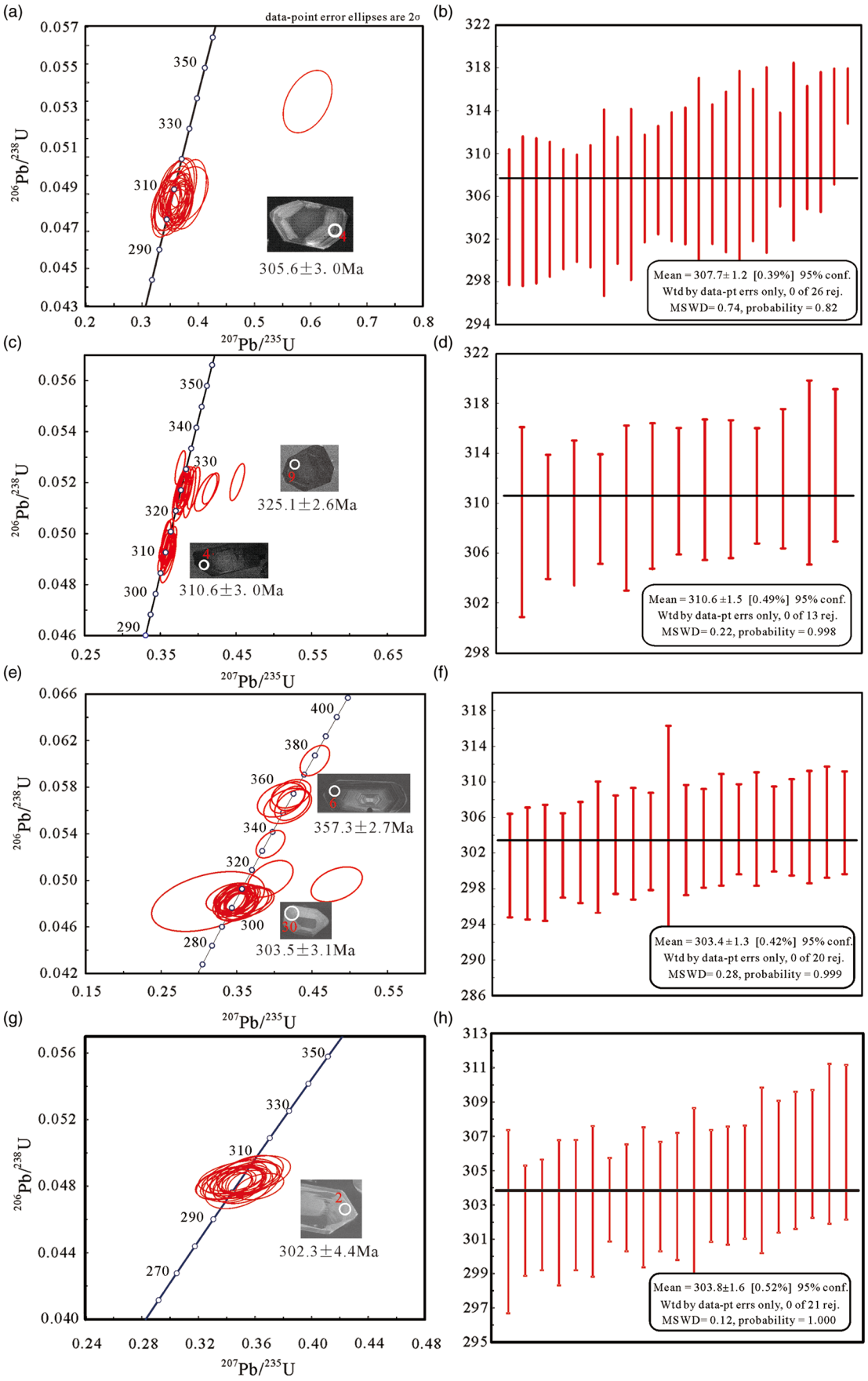

Fig. 4. (Colour online) Zircon concordia diagrams and weighting diagrams for the four igneous rock samples in the Daheyan region.

https://doi.org/10.1017/S001675681900075X Published online by Cambridge University Press

Table 1. LA-ICP-MS U–Pb data on zircons from the Daheyan intrusion

										$^{207}Pb/^{206}Pb$		$^{207}Pb/^{235}U$		$^{206}Pb/^{238}U$	
Sample no.	Th (10^{-6})	U (10^{-6})	Th/U	$^{207}Pb/^{206}Pb$	1σ	$^{207}Pb/^{235}U$	1σ	$^{206}Pb/^{238}U$	1σ	Age (Ma)	1σ	Age (Ma)	1σ	Age (Ma)	1σ
D01-01	46.2	127.7	0.36	0.0555	0.0016	0.3663	0.0100	0.0484	0.0006	433	66	317	7	305	4
D01-02	38.3	98.6	0.39	0.0526	0.0018	0.3506	0.0123	0.0486	0.0007	312	79	305	9	306	4
D01-03	100.4	166.1	0.60	0.0813	0.0027	0.5944	0.0177	0.0540	0.0007	1229	64	474	11	339	4
D01-04	66.8	151.0	0.44	0.0558	0.0013	0.3702	0.0085	0.0485	0.0005	444	52	320	6	306	3
D01-05	61.7	134.9	0.46	0.0565	0.0023	0.3795	0.0154	0.0490	0.0006	473	92	327	11	308	4
D01-06	77.5	168.8	0.46	0.0540	0.0016	0.3646	0.0116	0.0492	0.0007	370	68	316	9	309	4
D01-07	52.2	136.2	0.38	0.0530	0.0020	0.3531	0.0129	0.0485	0.0007	331	84	307	10	305	4
D01-08	56.9	130.5	0.44	0.0527	0.0014	0.3546	0.0093	0.0489	0.0005	318	59	308	7	308	3
D01-09	56.8	130.1	0.44	0.0665	0.0017	0.4507	0.0107	0.0497	0.0004	821	52	378	7	313	3
D01-10	66.8	156.7	0.43	0.0585	0.0025	0.3783	0.0137	0.0473	0.0010	549	94	326	10	298	6
D01-11	52.9	125.5	0.42	0.0553	0.0012	0.3698	0.0080	0.0489	0.0005	424	49	320	6	308	3
D01-12	69.7	206.7	0.34	0.0542	0.0010	0.3669	0.0070	0.0492	0.0004	378	43	317	5	309	2
D01-13	54.4	100.2	0.54	0.0733	0.0026	0.4888	0.0161	0.0489	0.0005	1022	71	404	11	308	3
D01-14	60.8	138.9	0.44	0.0521	0.0012	0.3488	0.0082	0.0487	0.0004	291	53	304	6	307	3
D01-15	69.8	145.2	0.48	0.0549	0.0011	0.3649	0.0073	0.0484	0.0004	410	46	316	5	305	2
D01-16	83.3	174.2	0.48	0.0522	0.0015	0.3413	0.0095	0.0479	0.0005	296	68	298	7	302	3
D01-17	75.5	165.8	0.46	0.0551	0.0014	0.3663	0.0088	0.0484	0.0005	416	55	317	7	305	3
D01-18	27.6	70.9	0.39	0.0919	0.0049	0.6197	0.0344	0.0489	0.0007	1466	102	490	22	308	5
D01-19	62.2	156.0	0.40	0.0525	0.0016	0.3573	0.0110	0.0494	0.0005	306	70	310	8	311	3
D01-20	44.0	121.4	0.36	0.0540	0.0014	0.3585	0.0089	0.0485	0.0005	369	58	311	7	305	3
D01-21	60.6	152.1	0.40	0.0546	0.0013	0.3609	0.0081	0.0482	0.0004	397	52	313	6	303	3
D01-22	95.7	249.1	0.38	0.0571	0.0021	0.3824	0.0130	0.0490	0.0008	495	80	329	10	308	5
D01-23	67.8	148.2	0.46	0.0551	0.0015	0.3651	0.0096	0.0484	0.0005	415	62	316	7	305	3
D01-24	49.6	122.6	0.40	0.0544	0.0021	0.3649	0.0131	0.0493	0.0007	388	87	316	10	310	4
D01-25	75.0	164.8	0.46	0.0745	0.0018	0.5040	0.0106	0.0497	0.0004	1055	48	414	7	313	3
D01-26	90.7	187.5	0.48	0.0523	0.0015	0.3469	0.0097	0.0483	0.0005	300	66	302	7	304	3
D01-27	74.3	167.9	0.44	0.0535	0.0014	0.3582	0.0093	0.0489	0.0004	349	61	311	7	308	3
D01-28	57.1	131.0	0.44	0.0727	0.0021	0.4939	0.0148	0.0494	0.0005	1007	59	408	10	311	3
D01-29	56.8	134.4	0.42	0.0514	0.0016	0.3417	0.0104	0.0484	0.0006	259	71	298	8	305	3
D01-30	63.1	148.5	0.43	0.0540	0.0015	0.3627	0.0098	0.0491	0.0006	371	65	314	7	309	4
D02-01	1605.9	1765.5	0.91	0.0533	0.0007	0.3817	0.0056	0.0518	0.0004	342	28	328	4	326	2
D02-02	250.3	487.2	0.51	0.0535	0.0008	0.3815	0.0065	0.0516	0.0004	350	34	328	5	324	2
D02-03	1881.6	2376.7	0.79	0.0531	0.0008	0.3608	0.0051	0.0494	0.0005	331	32	313	4	311	3
D02-04	1024.1	1426.7	0.72	0.0530	0.0005	0.3801	0.0048	0.0520	0.0004	328	23	327	4	327	3
D02-05	1827.1	2419.3	0.76	0.0551	0.0006	0.3940	0.0055	0.0518	0.0005	416	25	337	4	325	3
D02-06	2599.8	5948.3	0.44	0.0540	0.0006	0.3840	0.0051	0.0516	0.0004	370	23	330	4	324	2
D02-07	1448.7	3767.9	0.38	0.0530	0.0004	0.3786	0.0046	0.0517	0.0004	329	18	326	3	325	3
D02-08	1464.0	2591.0	0.57	0.0628	0.0006	0.4516	0.0065	0.0520	0.0005	701	21	378	5	327	3
D02-09	2498.6	2254.0	1.11	0.0584	0.0009	0.4164	0.0073	0.0518	0.0004	544	33	353	5	325	2
D02-10	318.0	573.1	0.55	0.0527	0.0006	0.3579	0.0046	0.0492	0.0004	317	27	311	3	310	2
D02-11	188.8	1393.3	0.14	0.0534	0.0006	0.3801	0.0053	0.0516	0.0006	346	27	327	4	325	4
D02-12	1750.1	1892.3	0.92	0.0574	0.0012	0.4102	0.0099	0.0516	0.0005	506	47	349	7	324	3

(*Continued*)

https://doi.org/10.1017/S001675681900075X Published online by Cambridge University Press

Table 1. (*Continued*)

										$^{207}Pb/^{206}Pb$		$^{207}Pb/^{235}U$		$^{206}Pb/^{238}U$	
Sample no.	Th (10^{-6})	U (10^{-6})	Th/U	$^{207}Pb/^{206}Pb$	1σ	$^{207}Pb/^{235}U$	1σ	$^{206}Pb/^{238}U$	1σ	Age (Ma)	1σ	Age (Ma)	1σ	Age (Ma)	1σ
D02-13	2067.5	2919.5	0.71	0.0527	0.0005	0.3574	0.0037	0.0491	0.0005	316	22	310	3	309	3
D02-14	2114.6	2495.8	0.85	0.0529	0.0006	0.3613	0.0043	0.0494	0.0004	325	26	313	3	311	3
D02-15	813.5	3269.5	0.25	0.0529	0.0007	0.3628	0.0058	0.0496	0.0005	325	31	314	4	312	3
D02-16	878.0	1141.1	0.77	0.0714	0.0022	0.5581	0.0246	0.0541	0.0006	970	62	450	16	340	4
D02-17	1987.0	2173.1	0.91	0.0547	0.0008	0.3888	0.0053	0.0516	0.0007	398	31	333	4	324	4
D02-18	1755.4	2326.1	0.75	0.0524	0.0007	0.3592	0.0056	0.0497	0.0006	302	31	312	4	312	4
D02-19	464.7	830.2	0.56	0.0531	0.0011	0.3780	0.0080	0.0516	0.0007	334	49	326	6	324	4
D02-20	2318.6	2207.8	1.05	0.0529	0.0005	0.3771	0.0041	0.0517	0.0004	322	23	325	3	325	3
D02-21	357.0	718.7	0.50	0.0527	0.0010	0.3571	0.0069	0.0491	0.0004	315	44	310	5	309	2
D02-22	1548.4	1765.6	0.88	0.0528	0.0005	0.3772	0.0042	0.0518	0.0005	320	20	325	3	325	3
D02-23	1453.2	2001.7	0.73	0.0532	0.0011	0.3603	0.0069	0.0490	0.0006	338	45	312	5	308	4
D02-24	280.0	584.1	0.48	0.0522	0.0007	0.3567	0.0055	0.0495	0.0004	294	32	310	4	311	2
D03-01	37.7	73.1	0.52	0.0716	0.0021	0.4836	0.0138	0.0496	0.0006	975	59	401	9	312	4
D03-02	70.8	105.4	0.67	0.0554	0.0018	0.3678	0.0130	0.0481	0.0005	429	74	318	10	303	3
D03-03	137.6	386.9	0.36	0.0528	0.0010	0.3527	0.0074	0.0484	0.0004	319	44	307	6	305	3
D03-04	139.7	190.6	0.73	0.0527	0.0010	0.3509	0.0072	0.0484	0.0004	316	44	305	5	305	3
D03-05	152.3	204.1	0.75	0.0526	0.0010	0.3508	0.0072	0.0484	0.0004	311	44	305	5	305	2
D03-06	38.6	72.5	0.53	0.0529	0.0015	0.3509	0.0104	0.0482	0.0005	326	65	305	8	303	3
D03-07	40.4	90.0	0.45	0.0523	0.0016	0.3427	0.0098	0.0480	0.0005	299	68	299	7	302	3
D03-08	55.0	89.6	0.61	0.0529	0.0016	0.3484	0.0109	0.0477	0.0005	326	70	304	8	301	3
D03-09	29.9	66.4	0.45	0.0527	0.0016	0.4096	0.0128	0.0568	0.0006	316	70	349	9	356	4
D03-10	48.0	135.5	0.35	0.0536	0.0013	0.4234	0.0107	0.0574	0.0005	355	57	358	8	360	3
D03-11	222.7	422.0	0.53	0.0545	0.0008	0.4542	0.0079	0.0602	0.0005	393	34	380	6	377	3
D03-12	36.7	72.1	0.51	0.0529	0.0019	0.3491	0.0120	0.0485	0.0005	323	82	304	9	305	3
D03-13	65.9	103.2	0.64	0.0515	0.0021	0.3423	0.0134	0.0485	0.0005	262	92	299	10	305	3
D03-14	37.1	95.6	0.39	0.0551	0.0014	0.4258	0.0101	0.0564	0.0005	414	55	360	7	354	3
D03-15	56.7	147.8	0.38	0.0552	0.0020	0.3654	0.0128	0.0482	0.0005	419	82	316	10	304	3
D03-16	29.4	56.6	0.52	0.0550	0.0021	0.3602	0.0131	0.0481	0.0006	413	84	312	10	303	4
D03-17	28.0	57.7	0.49	0.0540	0.0016	0.4170	0.0126	0.0564	0.0006	372	68	354	9	354	4
D03-18	100.9	165.4	0.61	0.0512	0.0012	0.3413	0.0083	0.0484	0.0005	248	55	298	6	305	3
D03-19	77.4	123.9	0.62	0.0521	0.0013	0.3431	0.0082	0.0481	0.0004	289	57	299	6	303	3
D03-20	46.8	88.2	0.53	0.0541	0.0018	0.3511	0.0108	0.0478	0.0005	376	73	306	8	301	3
D03-21	44.4	73.8	0.60	0.0540	0.0016	0.3522	0.0109	0.0478	0.0005	371	69	306	8	301	3
D03-22	78.5	158.7	0.49	0.0523	0.0013	0.3452	0.0080	0.0482	0.0004	300	55	301	6	303	3
D03-23	45.7	156.5	0.29	0.0534	0.0012	0.4194	0.0098	0.0571	0.0006	344	49	356	7	358	3
D03-24	60.0	98.0	0.61	0.0530	0.0015	0.3504	0.0097	0.0484	0.0005	328	63	305	7	305	3
D03-25	125.3	182.9	0.69	0.0544	0.0011	0.3956	0.0080	0.0531	0.0005	388	45	338	6	333	3
D03-26	41.4	71.8	0.58	0.0473	0.0049	0.3122	0.0306	0.0482	0.0011	66	245	276	24	303	6
D03-27	47.9	89.6	0.53	0.0581	0.0020	0.3961	0.0126	0.0501	0.0006	532	75	339	9	315	4
D03-28	151.2	207.5	0.73	0.0531	0.0010	0.3493	0.0065	0.0479	0.0004	332	42	304	5	302	2
D03-29	47.9	82.6	0.58	0.0530	0.0018	0.3518	0.0121	0.0484	0.0005	328	76	306	9	305	3
D03-30	87.0	374.7	0.23	0.0536	0.0008	0.4221	0.0073	0.0570	0.0004	355	35	358	5	357	3

https://doi.org/10.1017/S001675681900075X Published online by Cambridge University Press

Table 1. (*Continued*)

										$^{207}Pb/^{206}Pb$		$^{207}Pb/^{235}U$		$^{206}Pb/^{238}U$	
Sample no.	Th (10^{-6})	U (10^{-6})	Th/U	$^{207}Pb/^{206}Pb$	1σ	$^{207}Pb/^{235}U$	1σ	$^{206}Pb/^{238}U$	1σ	Age (Ma)	1σ	Age (Ma)	1σ	Age (Ma)	1σ
D04-01	66.4	100.1	0.66	0.0524	0.0030	0.3485	0.0187	0.0485	0.0007	302	130	304	14	306	4
D04-02	52.6	94.1	0.56	0.0522	0.0022	0.3457	0.0148	0.0482	0.0007	293	95	301	11	303	4
D04-03	74.3	160.6	0.46	0.0534	0.0013	0.3529	0.0090	0.0483	0.0006	346	57	307	7	304	3
D04-04	65.6	104.2	0.63	0.0637	0.0024	0.4160	0.0139	0.0481	0.0006	731	79	353	10	303	4
D04-05	86.2	148.2	0.58	0.0529	0.0024	0.3486	0.0157	0.0480	0.0009	324	103	304	12	302	5
D04-06	100.7	128.9	0.78	0.0528	0.0015	0.3494	0.0104	0.0482	0.0006	319	65	304	8	303	4
D04-07	41.7	96.2	0.43	0.0556	0.0018	0.3633	0.0113	0.0480	0.0005	438	72	315	8	302	3
D04-08	48.7	99.4	0.49	0.0515	0.0024	0.3425	0.0162	0.0482	0.0007	264	109	299	12	303	4
D04-09	53.2	95.6	0.56	0.0530	0.0021	0.3462	0.0129	0.0478	0.0006	330	92	302	10	301	4
D04-10	55.5	84.2	0.66	0.0515	0.0021	0.3382	0.0130	0.0481	0.0006	265	91	296	10	303	4
D04-11	40.1	82.9	0.48	0.0519	0.0021	0.3473	0.0140	0.0486	0.0006	282	95	303	11	306	4
D04-12	59.1	113.0	0.52	0.0533	0.0025	0.3520	0.0156	0.0485	0.0008	340	108	306	12	305	5
D04-13	33.5	59.8	0.56	0.0533	0.0018	0.3529	0.0120	0.0483	0.0005	342	75	307	9	304	3
D04-14	57.8	107.0	0.54	0.0515	0.0018	0.3400	0.0123	0.0480	0.0005	261	82	297	9	302	3
D04-15	79.9	178.7	0.45	0.0531	0.0022	0.3566	0.0154	0.0487	0.0008	333	93	310	12	307	5
D04-16	48.0	99.3	0.48	0.0533	0.0024	0.3589	0.0173	0.0487	0.0007	343	104	311	13	307	5
D04-17	95.0	144.2	0.66	0.0555	0.0014	0.4275	0.0114	0.0559	0.0005	432	58	361	8	351	3
D04-18	234.7	361.3	0.65	0.0542	0.0011	0.3885	0.0087	0.0518	0.0006	380	44	333	6	326	3
D04-19	50.2	93.2	0.54	0.0538	0.0019	0.3541	0.0124	0.0478	0.0005	362	78	308	9	301	3
D04-20	56.7	130.5	0.43	0.0543	0.0016	0.3866	0.0103	0.0520	0.0006	385	64	332	8	327	3
D04-21	63.7	124.3	0.51	0.0538	0.0023	0.3578	0.0140	0.0485	0.0006	365	94	311	10	305	4
D04-22	51.8	87.4	0.59	0.0515	0.0026	0.3301	0.0156	0.0469	0.0007	263	116	290	12	296	4
D04-23	89.5	176.3	0.51	0.0533	0.0023	0.3539	0.0156	0.0482	0.0008	343	99	308	12	304	5
D04-24	68.2	165.9	0.41	0.0593	0.0013	0.4666	0.0095	0.0575	0.0005	578	49	389	7	361	3
D04-25	52.0	113.2	0.46	0.0536	0.0026	0.3623	0.0177	0.0488	0.0008	355	112	314	13	307	5
D04-26	144.4	257.5	0.56	0.0523	0.0010	0.3470	0.0069	0.0482	0.0004	298	45	302	5	303	2
D04-27	127.6	177.2	0.72	0.0537	0.0014	0.3542	0.0088	0.0482	0.0005	359	57	308	7	303	3
D04-28	52.7	91.5	0.58	0.0526	0.0017	0.3444	0.0108	0.0482	0.0005	310	75	300	8	303	3
D04-29	41.9	72.4	0.58	0.0520	0.0022	0.3441	0.0142	0.0483	0.0005	288	95	300	11	304	3
D04-30	113.1	170.9	0.66	0.0527	0.0018	0.3484	0.0116	0.0481	0.0007	318	79	304	9	303	4

Twenty-five analyses of sample D02 from diorite display $^{176}Hf/^{177}Hf$ ratios of 0.0012–0.0119 and $\epsilon_{Hf}(t)$ values of +4.3 to +14.7. The corresponding T_{DM1} is *c.* 362–941 Ma and the corresponding T_{DM2} is *c.* 389–1048 Ma.

The 19 analyses of sample D03 from granodiorite display $^{176}Hf/^{177}Hf$ ratios of 0.0007–0.0032 and $\epsilon_{Hf}(t)$ values of +7.6 to +15.6. The corresponding T_{DM1} is *c.* 316–702 Ma, whereas the T_{DM2} is *c.* 322–872 Ma.

Twenty-five *in situ* Hf isotopic analyses of sample D04 from monzonite exhibit variable initial Hf isotopic compositions, resulting in $^{176}Hf/^{177}Hf$ ratios of 0.0006–0.0016 and $\epsilon_{Hf}(t)$ of +11.0 to +15.8. T_{DM1} values are *c.* 311–502 Ma and T_{DM2} values are *c.* 313–617 Ma.

5. Discussion

5.a. Timing of magmatism in the Daheyan area, Bogda Mountains

The LA-ICP-MS zircon U–Pb ages for the syenogranite, diorite, granodiorite and monzonite in the Daheyan area are 307.7 ± 1.2, 310.6 ± 1.5, 303.3 ± 1.3 and 303.8 ± 1.6 Ma, respectively, which are consistent with some volcanic rocks in the Bogda Mountains. Wali *et al.* (2018) reported LA-ICP-MS zircon U–Pb ages of 298 ± 8 Ma for rhyolite of the Daheyan area, and Xie *et al.* (2016*b*) reported a LA-ICP-MS zircon U–Pb age of 311 ± 2 Ma for dacite ignimbrite from Baiyanggou, Bogda Mountains. The similarity between these ages shows they were derived from the same late Carboniferous magmatic events.

https://doi.org/10.1017/S001675681900075X Published online by Cambridge University Press

Table 2. Major (%) and trace element (μg g^{-1}) data for the intrusion in the Daheyan area. LREE – light rare earth element; HREE – heavy rare earth element

Sample No.	D-1	D-2	D-3	D-4	D-5	D-6	D-7	D-8	D-9	D-10	D-11	D-12
Rock type	Syenogranite				Monzonite	Diorite		Granodiorite				
SiO_2 (%)	70.37	70.87	70.45	70.18	61.50	61.22	61.70	68.67	68.61	68.59	68.14	68.22
TiO_2 (%)	0.38	0.42	0.44	0.43	0.96	0.95	0.97	0.27	0.26	0.24	0.24	0.27
Al_2O_3 (%)	13.34	13.42	13.43	13.42	14.68	14.67	14.90	15.89	15.87	15.59	15.54	15.92
TFe_2O_3 (%)	3.48	3.59	3.70	3.64	7.61	7.14	7.08	3.19	3.16	3.48	3.01	3.39
MnO (%)	0.06	0.06	0.06	0.06	0.09	0.10	0.10	0.12	0.12	0.17	0.18	0.11
MgO (%)	0.32	0.38	0.43	0.42	1.82	1.84	1.82	0.76	0.80	0.73	0.74	0.78
CaO (%)	0.94	0.92	1.14	1.08	3.74	4.22	4.22	1.60	1.44	1.12	1.34	1.26
Na_2O (%)	4.45	4.60	4.94	4.85	5.42	7.55	7.76	5.59	5.66	5.45	5.53	6.14
K_2O (%)	5.05	4.86	4.45	4.52	2.68	0.42	0.41	2.82	2.85	3.11	3.03	2.60
P_2O_5 (%)	0.06	0.07	0.07	0.07	0.32	0.32	0.32	0.15	0.15	0.15	0.15	0.15
LOI (%)	0.69	0.60	0.70	0.57	1.04	0.97	1.04	1.09	1.14	1.12	1.26	1.26
A/CNK	0.92	0.92	0.89	0.90	0.78	0.71	0.71	1.05	1.06	1.08	1.05	1.05
Mg no.	15.41	17.33	18.71	18.60	32.15	33.80	33.74	32.06	33.40	29.36	32.75	31.31
Cr (μg g^{-1})	20.00	20.00	20.00	20.00	10.00	20.00	10.00	10.00	20.00	10.00	10.00	10.00
Ga (μg g^{-1})	16.25	14.80	15.55	15.65	18.25	17.25	18.05	15.45	15.55	15.65	15.50	16.15
Rb (μg g^{-1})	154.0	139.5	130.5	132.5	72.0	12.9	13.2	95.1	98.0	109.0	113.0	92.4
Sr (μg g^{-1})	53.7	51.3	47.6	54.0	177.0	142.5	149.0	842	793	657	672	678
Y (μg g^{-1})	48.0	45.2	50.3	49.7	45.4	45.4	45.1	12.3	12.4	12.6	12.9	12.0
Zr (μg g^{-1})	492	482	465	482	285	324	310	169	161	176	156	173
Nb (μg g^{-1})	11.6	11.4	10.9	11.4	8.2	8.3	7.9	4.6	4.3	4.4	4.4	4.4
Cs (μg g^{-1})	1.89	1.15	0.78	0.82	0.61	0.21	0.21	2.65	2.77	7.41	6.41	3.42
Ba (μg g^{-1})	329	317	247	264	438	101.0	104.5	740	724	744	748	630
La (μg g^{-1})	30.1	26.9	26.9	27.4	27.9	24.6	21.3	21.1	21.5	23.2	21.5	22.2
Ce (μg g^{-1})	73.1	64.3	63.1	65.8	64.2	58.8	51.9	45.7	45.6	49.7	45.7	48.4
Pr (μg g^{-1})	8.73	7.95	7.75	8.02	7.91	7.31	6.67	5.48	5.28	5.75	5.36	5.53
Nd (μg g^{-1})	35.5	32.8	32.8	33.1	34.0	32.5	30.4	21.9	21.3	22.5	21.1	22.0
Sm (μg g^{-1})	8.00	7.51	7.72	7.51	7.69	7.77	7.41	3.80	3.83	4.01	3.86	3.80
Eu (μg g^{-1})	0.89	0.87	0.89	0.91	1.68	1.66	1.66	1.11	1.11	1.15	1.13	1.08
Gd (μg g^{-1})	7.78	7.54	7.58	7.68	7.98	8.28	7.59	3.05	3.00	3.09	2.93	3.04
Tb (μg g^{-1})	1.28	1.25	1.24	1.30	1.26	1.31	1.28	0.44	0.43	0.43	0.41	0.42
Dy (μg g^{-1})	8.52	8.37	8.43	8.44	7.90	8.29	8.00	2.52	2.50	2.43	2.43	2.41
Ho (μg g^{-1})	1.80	1.76	1.77	1.81	1.70	1.73	1.71	0.50	0.50	0.50	0.50	0.50
Er (μg g^{-1})	5.61	5.47	5.57	5.52	4.88	5.05	4.90	1.47	1.41	1.46	1.44	1.46
Tm (μg g^{-1})	0.86	0.86	0.84	0.85	0.75	0.78	0.76	0.24	0.22	0.22	0.23	0.23
Yb (μg g^{-1})	6.00	5.76	5.99	6.00	4.89	5.04	4.92	1.64	1.64	1.56	1.57	1.58
Lu (μg g^{-1})	0.98	0.94	0.96	0.96	0.76	0.81	0.78	0.26	0.27	0.28	0.27	0.26
Hf (μg g^{-1})	12.4	12.3	11.8	12.2	7.2	8.1	7.9	4.3	4.3	4.6	4.0	4.4
Ta (μg g^{-1})	0.78	0.70	0.73	0.73	0.48	0.46	0.50	0.26	0.26	0.28	0.28	0.26
Th (μg g^{-1})	13.15	12.55	12.70	12.80	7.00	6.91	6.84	6.74	6.67	6.85	6.76	6.71
U (μg g^{-1})	5.47	5.04	4.61	4.83	2.38	2.51	2.55	1.94	1.92	1.55	1.98	1.76
δEu	0.34	0.35	0.35	0.36	0.65	0.63	0.67	0.96	0.97	0.96	0.99	0.94
∑LREE/∑HREE	4.61	4.21	4.24	4.23	4.69	4.15	3.89	9.54	9.74	10.41	9.96	10.14
$(La/Yb)_N$	3.57	3.20	3.16	3.14	4.06	3.46	3.05	9.05	9.23	10.53	9.78	9.94

https://doi.org/10.1017/S001675681900075X Published online by Cambridge University Press

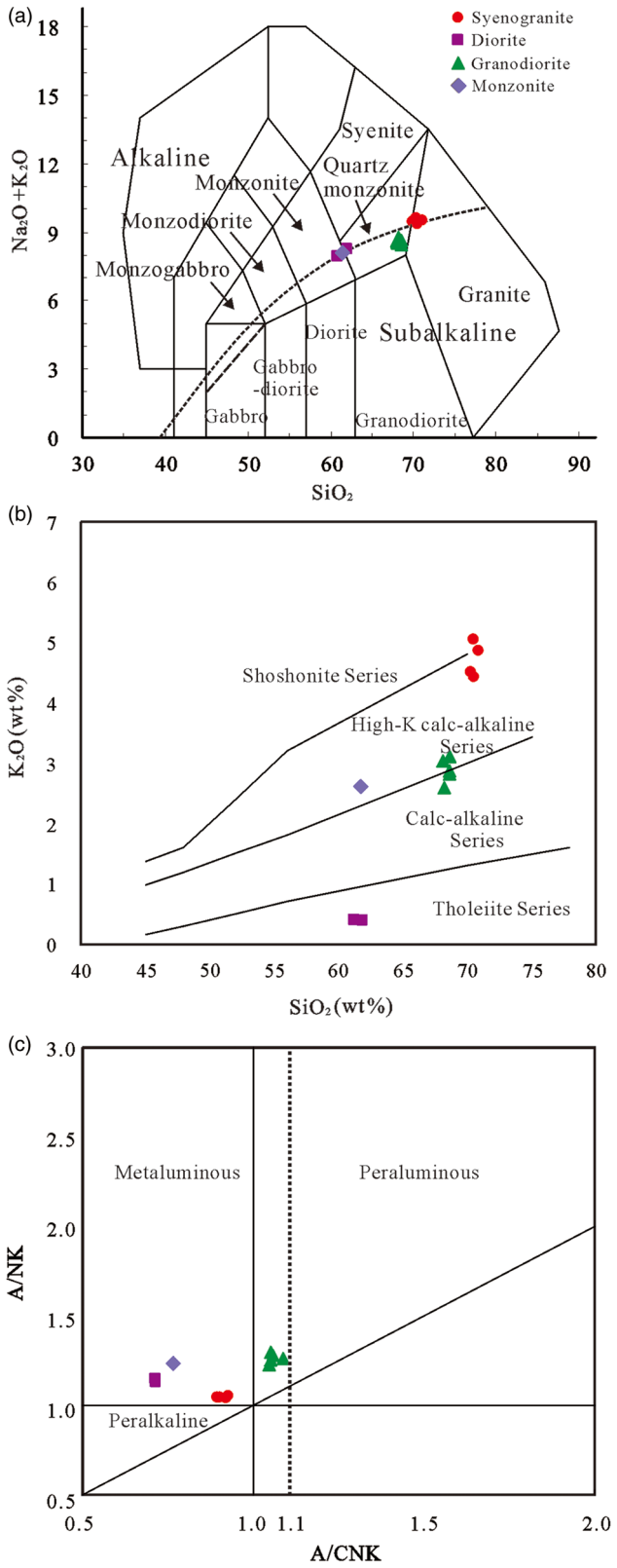

Fig. 5. (Colour online) (a) SiO_2 versus total alkali ($Na_2O + K_2O$) diagram; (b) SiO_2 versus K_2O diagram; and (c) A/CNK versus A/NK diagram for the Daheyan region. SiO_2 versus total alkali ($Na_2O + K_2O$), SiO_2 versus K_2O and A/CNK versus A/NK diagrams are from Middlemost (1994), Peccerillo & Taylor (1976) and Maniar & Piccoli (1989), respectively.

5.b. Petrogenesis of Upper Daheyan intrusions

5.b.1 Syenogranite

Syenogranite is enriched in SiO_2, slightly alkaline and low in Al_2O_3. It shows Ti, Ba, P and Sr negative anomalies, and displays clear negative Eu anomalies. This syenogranite has the chemical characteristics of A-type granite, which is characteristically enriched in SiO_2 and K_2O, shows Ba and Sr anomalies, and exhibits clearly negative Eu anomalies (Zhang *et al.* 2007). In addition, the value of $Zr + Ce + Nb + Y$ ranges from 589 to 624×10^{-6}, and approaches the related value of A-type granites ($>350 \times 10^{-6}$; Whalen *et al.* 1987). Moreover, we calculated the Zr saturation temperature of the syenogranite, revealing high crystallization temperatures (929–938°C, calculated from the equation of Watson & Harrison, 1983), which also suggests that syenogranite is an A-type granite. The zircon $\epsilon_{Hf}(t)$ values of the syenogranite vary from 11.2 to 14.4 (average of 12.8). On the $\epsilon_{Hf}(t)$ versus age diagram, all samples plot below the depleted mantle reference line and above the CHUR reference line (Fig. 7), suggesting that syenogranite was mainly derived from the melting of young crust with some contribution from mantle-derived materials. In addition, the two-stage Hf model ages (T_{DM2}) of syenogranite are 400–609 Ma, also indicating that syenogranite was mainly derived from the melting of juvenile crust.

5.b.2 Diorite

Chemical compositions of Daheyan diorite suggest they are tholeiite metaluminous diorites (Fig. 5b, c) that can be produced by partial melting of mafic lower crust (Jung *et al.* 2002). Moreover, experimental studies have shown that dehydration melting of crustal (basaltic and pelitic) rocks would produce low Mg (generally < 40) melts, regardless of the melting degrees (Patiño Douce & Johnston, 1991; Rapp & Watson, 1995). The Daheyan diorite has low Mg values of 33.7–33.8, also indicating it was mainly derived from crust rather than mantle material. Zircon $\epsilon_{Hf}(t)$ values of diorite are 4.3–14.7 with a wide range of values, indicating that the primary magma of the diorite was derived from multiple sources. On the $\epsilon_{Hf}(t)$ versus age diagram, all samples plot below the depleted mantle reference line and above the CHUR reference line (Fig. 7), suggesting that diorite was derived from the melting of young crust with some contributions from mantle-derived materials. In addition, the two-stage Hf model ages (T_{DM2}) of diorite vary from 389 to 1048 Ma. The T_{DM2} of diorite is older than that of syenogranite, which indicates that primary magma of diorite was derived from juvenile crust and some mixed mantle materials.

In brief, the studied syenogranite is an A-type granite, and the studied diorite is a low-Mg diorite with tholeiite and metaluminous features. The syenogranite and diorite both resulted from late Carboniferous magmatism with ages of 307.7 ± 1.2 Ma and 310.6 ± 1.5 Ma, respectively. On the other hand, samples of syenogranite and diorite have different trace-element patterns (Fig. 6) and diverse negative Eu anomalies; moreover, the diorite has a wider range of $\epsilon_{Hf}(t)$ values than the syenogranite. These features imply that syenogranite and diorite have disparate magma source characteristics; the primary magma of syenogranite was sourced from juvenile crust, while the primary magma of diorite was derived from juvenile crust and mixed mantle materials.

https://doi.org/10.1017/S001675681900075X Published online by Cambridge University Press

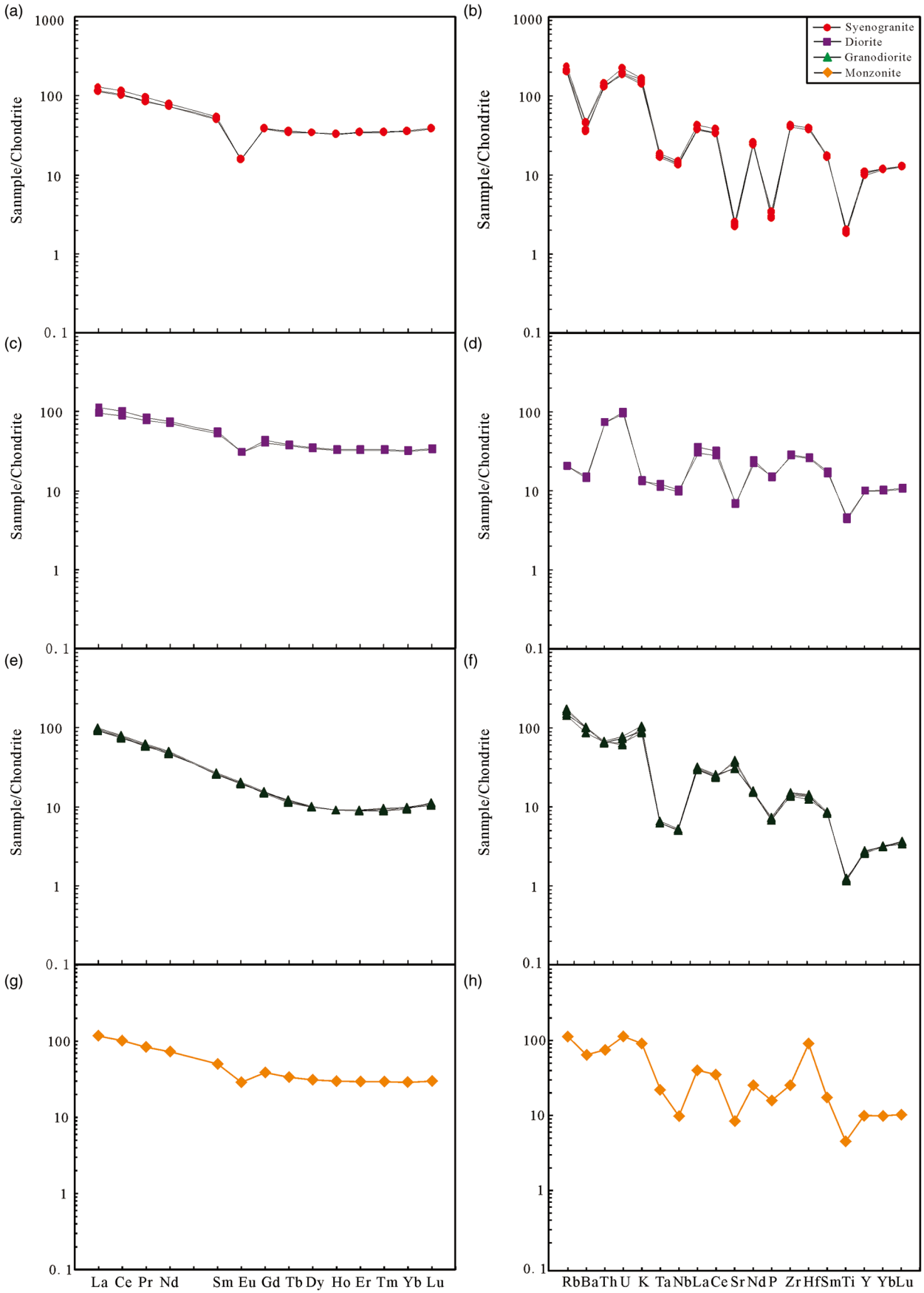

Fig. 6. (Colour online) Chondrite-normalized REE pattern and primitive-mantle-normalized spider diagrams of igneous rocks in Daheyan. Chondrite and primitive mantle values used for normalization are from Boynton (1984) and Sun & McDonough (1989).

https://doi.org/10.1017/S001675681900075X Published online by Cambridge University Press

Table 3. Zircon Lu–Hf isotopic data for the Daheyan intrusion from the Bogda orogenic belt

Sample spot	$^{176}Lu/^{177}Hf$	$^{176}Yb/^{177}Hf$	$^{176}Hf/^{177}Hf$	$^{176}Hf/^{177}Hf$ (t)	ϵ_{Hf} (0)	ϵ_{Hf} (t)	σ	T_{DM1}	T_{DM2}	f_S
D01-01	0.001169	0.033947	0.282911	0.282904	4.92	11.38	0.85	485	591	–0.96
D01-02	0.000965	0.027556	0.282963	0.282957	6.75	13.30	0.88	409	470	–0.97
D01-04	0.001851	0.054888	0.282975	0.282964	7.18	13.53	0.92	401	455	–0.94
D01-05	0.001663	0.047698	0.282995	0.282985	7.89	14.33	0.92	371	406	–0.95
D01-07	0.001061	0.029391	0.282904	0.282898	4.67	11.17	0.85	494	605	–0.97
D01-08	0.001478	0.043489	0.282988	0.282979	7.64	14.12	0.88	379	419	–0.96
D01-09	0.001782	0.053809	0.282907	0.282897	4.77	11.28	1.03	499	604	–0.95
D01-10	0.001672	0.050493	0.282954	0.282945	6.44	12.66	0.85	430	504	–0.95
D01-11	0.000944	0.026464	0.282963	0.282958	6.75	13.34	0.67	409	469	–0.97
D01-12	0.001015	0.028261	0.282967	0.282961	6.9	13.5	0.74	404	460	–0.97
D01-14	0.001344	0.040314	0.28294	0.282932	5.94	12.42	0.81	446	527	–0.96
D01-16	0.001446	0.04116	0.282915	0.282907	5.06	11.41	0.96	483	587	–0.96
D01-17	0.002256	0.067907	0.282939	0.282926	5.91	12.16	1.06	459	542	–0.93
D01-18	0.00089	0.025546	0.282953	0.282948	6.40	13.00	0.74	422	491	–0.97
D01-19	0.001659	0.048788	0.28297	0.28296	7.00	13.51	0.88	407	460	–0.95
D01-20	0.001611	0.048571	0.282934	0.282925	5.73	12.12	0.85	458	545	–0.95
D01-22	0.001006	0.028824	0.282924	0.282918	5.38	11.96	0.92	465	557	–0.97
D01-23	0.001066	0.031259	0.282982	0.282976	7.43	13.92	0.78	383	429	–0.97
D01-24	0.001455	0.04321	0.282937	0.282929	5.84	12.36	0.85	452	533	–0.96
D01-25	0.001182	0.033354	0.282957	0.28295	6.54	13.18	0.78	420	483	–0.96
D01-26	0.002007	0.060525	0.282947	0.282936	6.19	12.48	0.96	444	521	–0.94
D01-27	0.001306	0.038467	0.282922	0.282914	5.30	11.81	0.85	472	566	–0.96
D01-28	0.001201	0.035916	0.282994	0.282987	7.85	14.44	0.96	367	400	–0.96
D01-29	0.000867	0.024991	0.282972	0.282967	7.07	13.60	0.78	395	449	–0.97
D02-01	0.010934	0.359396	0.282763	0.282699	–0.32	4.27	1.20	941	1048	–0.67
D02-02	0.004809	0.145957	0.283001	0.282972	8.10	14.23	0.96	396	426	–0.86
D02-03	0.002802	0.088524	0.282893	0.282876	4.28	10.81	0.96	534	643	–0.92
D02-04	0.003333	0.108166	0.282899	0.28288	4.49	10.64	0.99	533	643	–0.9
D02-05	0.003482	0.11434	0.282944	0.282923	6.08	12.52	0.92	467	536	–0.9
D02-06	0.004523	0.145754	0.282985	0.282957	7.53	13.72	0.88	417	458	–0.86
D02-07	0.003867	0.123391	0.282937	0.282913	5.84	12.16	0.88	483	558	–0.88
D02-08	0.002424	0.07442	0.282999	0.282984	8.03	14.65	0.96	372	398	–0.93
D02-09	0.003847	0.125043	0.28291	0.282887	4.88	11.21	0.99	524	618	–0.88
D02-10	0.004057	0.123742	0.282978	0.282953	7.29	13.6	0.99	423	467	–0.88
D02-11	0.003097	0.095016	0.282895	0.282876	4.35	10.84	1.03	536	642	–0.91
D02-12	0.003127	0.106088	0.282946	0.282927	6.15	12.74	1.06	460	524	–0.91
D02-13	0.003682	0.117823	0.282936	0.282915	5.80	11.86	1.03	482	565	–0.89
D02-14	0.001216	0.035631	0.282978	0.282971	7.29	14.17	0.92	390	429	–0.96
D02-15	0.003776	0.124535	0.282923	0.2829	5.34	11.67	0.81	503	588	–0.89
D02-16	0.011901	0.410258	0.282822	0.282753	1.77	6.13	0.96	858	929	–0.64
D02-17	0.006606	0.219407	0.282915	0.282877	5.06	10.54	0.81	561	650	–0.8
D02-18	0.001805	0.054881	0.283002	0.282991	8.13	14.65	0.92	362	389	–0.95
D02-19	0.003653	0.11799	0.282883	0.282862	3.93	10.04	0.85	563	683	–0.89

(*Continued*)

https://doi.org/10.1017/S001675681900075X Published online by Cambridge University Press

Table 3. (*Continued*)

Sample spot	$^{176}Lu/^{177}Hf$	$^{176}Yb/^{177}Hf$	$^{176}Hf/^{177}Hf$	$^{176}Hf/^{177}Hf$ (t)	ϵ_{Hf} (0)	ϵ_{Hf} (t)	σ	T_{DM1}	T_{DM2}	f_S
D02-20	0.003113	0.105123	0.282969	0.282949	6.97	13.74	0.88	425	468	−0.91
D02-21	0.00599	0.198345	0.282893	0.282857	4.28	10.13	0.81	587	686	−0.82
D02-22	0.003055	0.096276	0.282936	0.282918	5.80	12.05	0.96	474	555	−0.91
D02-23	0.003487	0.113356	0.282898	0.282878	4.46	10.58	0.92	537	647	−0.89
D02-24	0.005062	0.171596	0.282869	0.282838	3.43	9.48	1.06	609	728	−0.85
D02-25	0.004498	0.151103	0.282891	0.282864	4.21	10.39	0.88	564	670	−0.86
D03-02	0.000893	0.023446	0.282901	0.282896	4.56	11.05	0.88	496	611	−0.97
D03-03	0.002017	0.048746	0.283035	0.283023	9.30	15.6	0.74	316	322	−0.94
D03-06	0.001106	0.029353	0.282935	0.282929	5.76	12.22	0.85	451	537	−0.97
D03-07	0.000906	0.022296	0.282983	0.282978	7.46	13.93	0.96	380	427	−0.97
D03-08	0.000841	0.022468	0.282913	0.282908	4.99	11.43	0.92	478	585	−0.97
D03-10	0.003237	0.09247	0.282786	0.282764	0.50	7.64	1.17	702	872	−0.9
D03-11	0.002266	0.059277	0.282964	0.282948	6.79	14.53	0.81	422	447	−0.93
D03-12	0.000969	0.025414	0.282977	0.282971	7.25	13.78	0.92	389	439	−0.97
D03-14	0.002291	0.059987	0.282906	0.282891	4.74	12	0.81	508	590	−0.93
D03-15	0.001245	0.029372	0.2829	0.282893	4.53	10.96	0.81	502	618	−0.96
D03-16	0.000787	0.019977	0.282962	0.282958	6.72	13.22	0.88	409	472	−0.98
D03-18	0.000817	0.019562	0.282954	0.282949	6.44	12.98	0.88	420	489	−0.98
D03-19	0.000822	0.022926	0.282949	0.282944	6.26	12.76	0.88	427	502	−0.98
D03-20	0.001103	0.03061	0.282939	0.282933	5.91	12.31	1.06	445	529	−0.97
D03-21	0.000723	0.020192	0.28289	0.282886	4.17	10.65	0.81	509	635	−0.98
D03-22	0.000706	0.01982	0.282999	0.282995	8.03	14.56	0.92	355	387	−0.98
D03-23	0.001763	0.050187	0.282941	0.282929	5.98	13.44	0.92	450	501	−0.95
D03-24	0.001438	0.04134	0.2829	0.282892	4.53	10.95	0.88	505	619	−0.96
D03-26	0.000997	0.027826	0.282961	0.282955	6.68	13.16	0.81	412	477	−0.97
D04-1-01	0.000894	0.024107	0.282991	0.282986	7.74	14.29	0.92	369	406	−0.97
D04-1-02	0.001057	0.028187	0.282979	0.282973	7.32	13.78	0.92	387	437	−0.97
D04-1-03	0.001076	0.028943	0.283014	0.283008	8.56	15.04	0.81	338	357	−0.97
D04-1-04	0.000926	0.025998	0.282972	0.282967	7.07	13.56	0.67	396	451	−0.97
D04-1-06	0.001172	0.031203	0.283007	0.283	8.31	14.76	0.92	348	375	−0.96
D04-1-08	0.000611	0.016145	0.282983	0.28298	7.46	14.02	0.99	377	422	−0.98
D04-1-09	0.000964	0.02707	0.282955	0.28295	6.47	12.96	0.92	420	490	−0.97
D04-1-10	0.00086	0.023494	0.28298	0.282975	7.36	13.82	0.96	384	433	−0.97
D04-1-11	0.000942	0.025372	0.282997	0.282992	7.96	14.44	0.85	361	395	−0.97
D04-1-12	0.001106	0.029353	0.282943	0.282937	6.05	12.56	0.96	439	517	−0.97
D04-1-13	0.001119	0.031717	0.282981	0.282975	7.39	13.88	1.03	385	432	−0.97
D04-1-14	0.000731	0.019491	0.282997	0.282993	7.96	14.5	0.85	359	391	−0.98
D04-1-15	0.001279	0.034444	0.282949	0.282942	6.26	12.66	0.88	433	508	−0.96
D04-1-16	0.000931	0.026522	0.282938	0.282933	5.87	12.43	1.03	444	526	−0.97
D04-1-18	0.001639	0.039772	0.283036	0.283027	9.34	15.76	0.99	311	313	−0.95
D04-1-20	0.001174	0.033	0.282988	0.282981	7.64	14.58	0.99	376	404	−0.96
D04-1-21	0.001065	0.027108	0.283002	0.282996	8.13	14.64	0.78	355	384	−0.97
D04-1-22	0.000922	0.02483	0.282934	0.282929	5.73	12.06	0.78	450	541	−0.97

https://doi.org/10.1017/S001675681900075X Published online by Cambridge University Press

Table 3. (*Continued*)

Sample spot	$^{176}Lu/^{177}Hf$	$^{176}Yb/^{177}Hf$	$^{176}Hf/^{177}Hf$	$^{176}Hf/^{177}Hf$ (t)	ϵ_{Hf} (0)	ϵ_{Hf} (t)	σ	T_{DM1}	T_{DM2}	f_S
D04-1-23	0.001102	0.028893	0.282952	0.282946	6.37	12.83	1.03	426	498	−0.97
D04-1-25	0.000858	0.023543	0.282925	0.28292	5.41	12	0.78	462	554	−0.97
D04-1-26	0.000957	0.021443	0.28299	0.282985	7.71	14.19	0.92	371	411	−0.97
D04-1-27	0.001047	0.028284	0.282981	0.282975	7.39	13.86	0.99	384	432	−0.97
D04-1-28	0.000924	0.02374	0.282971	0.282966	7.04	13.53	0.81	397	453	−0.97
D04-1-29	0.000661	0.018376	0.282967	0.282963	6.90	13.46	0.71	400	458	−0.98
D04-1-30	0.001478	0.040072	0.282902	0.282894	4.60	10.96	0.81	502	617	−0.96

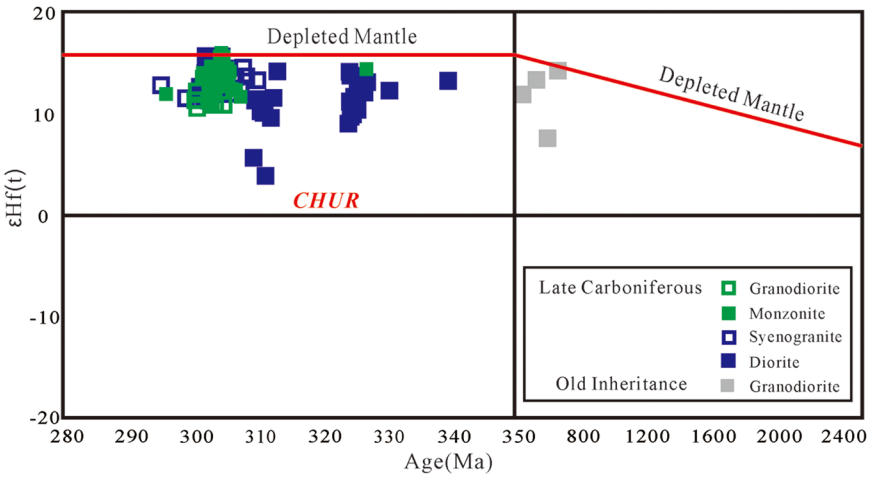

Fig. 7. (Colour online) Zircon U–Pb ages versus ϵ_{Hf}(t) plots for the upper Carboniferous magmatic rocks of the Daheyan region.

5.c. Petrogenesis of Lower Daheyan intrusions

5.c.1. Granodiorite

The granodiorite is characteristically enriched in SiO_2, has a high value of Na_2O and CaO, has relatively low K_2O values and is weakly peraluminous. Moreover, the value of Zr + Ce + Nb + Y ranges from 219 to 242×10^{-6}, below the lower limit of A-type granites (> 350×10^{-6}; Whalen *et al.* 1987). Moreover, we calculated the Zr saturation temperature of the granodiorite, revealing high crystallization temperatures (827–841°C; Watson & Harrison, 1983), significantly lower than that of typical A-type granites (> 900°C; Eby, 1990, 1992). As observed through petrographic microscopy, granodiorite contains hornblende minerals; the granodiorite is therefore an I-type granite (Chappell & White, 1992; Searle *et al.* 1997; Wu *et al.* 2007). Zircon ϵ_{Hf}(t) values from granodiorite range from 7.6 to 14.5 (Table 3). On the ϵ_{Hf}(t) versus age diagram, all samples plot below the depleted mantle reference line and above the CHUR reference line (Fig. 7), suggesting that granodiorite was mainly derived from melting of the crust with some contribution from mantle-derived materials. Devonian zircon xenocrysts in the Carboniferous granodiorite generally show positive ϵ_{Hf}(t) values; a fact that suggests the possible existence of Devonian juvenile crustal rocks in the basement of the Bogda Mountains. Moreover, two-stage Hf model ages (T_{DM2}) of granodiorite correspond to 427–872 Ma. These values are younger than those of basement rocks in the Cathaysia Block (1.8–2.2 Ga) (Chen *et al.* 1999), also indicating that the granodiorite was mainly derived from a juvenile crustal source.

5.c.2. Monzonite

Monzonite shows high Na_2O and CaO values. However, it has relatively low K_2O values, and is metaluminous. Moreover, we calculated the Zr saturation temperature of monzonite, which shows a high crystallization temperature (852°C; Watson & Harrison, 1983), significantly lower than that of typical A-type granites (> 900°C; Eby, 1990, 1992). In petrography, monzonite contains hornblende minerals; we therefore conclude that the monzonite is an I-type granite (Chappell & White, 1992; Searle *et al.* 1997; Wu *et al.* 2007).

Zircon ϵ_{Hf}(t) values of monzonite are 11.0–15.0 (Table 3). On the ϵ_{Hf}(t) versus age diagram, all samples plot below the depleted mantle reference line and above the CHUR reference line (Fig. 7), suggesting that monzonite was mainly derived from the melting of young crust with some contribution from mantle–derived materials. Moreover, two-stage Hf model ages (T_{DM2}) of monzonite vary from 357 to 617 Ma. These values are younger than those for basement rocks in the Cathaysia Block (1.8–2.2 Ga) (Chen *et al.* 1999), which also indicates that the monzonite was mainly derived from a Neoproterozoic crustal source.

Generally, samples of granodiorite and monzonite have similar LA-ICP-MS zircon U–Pb ages and Hf isotope data. However, they show differences in major- (e.g. Na_2O, CaO) and trace-element patterns, and in δEu values (Figs 5, 6). This suggests that granodiorite and monzonite have similar magma source characteristics but have experienced different degrees of fractional crystallization. In addition, the mineralization age of the Tonggou deposit is 303 ± 12 Ma based on Re–Os isotopic

https://doi.org/10.1017/S001675681900075X Published online by Cambridge University Press

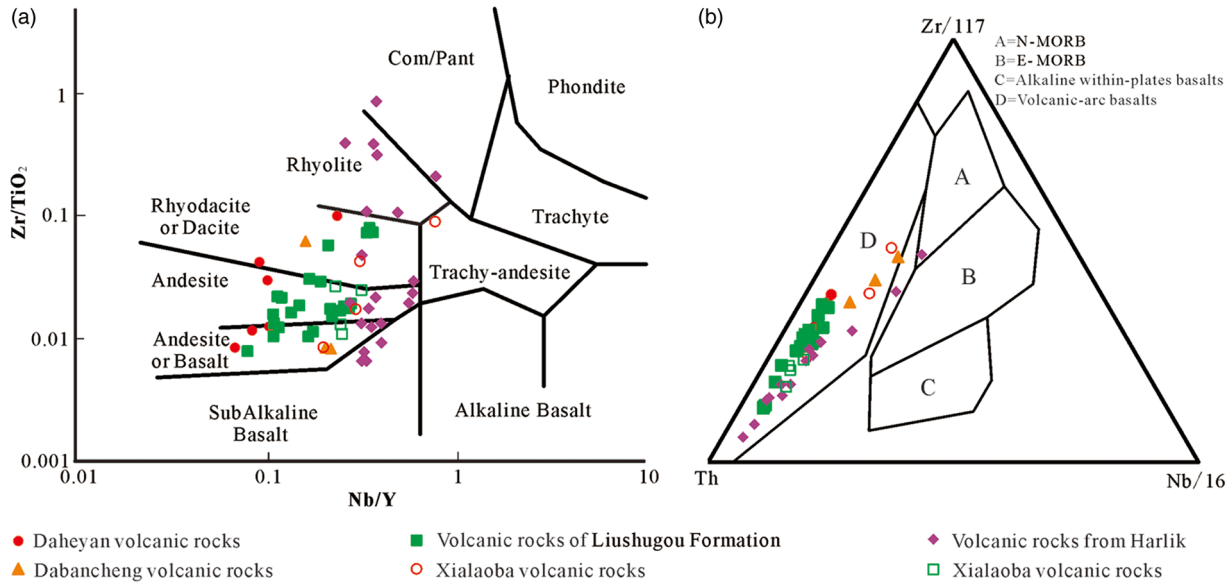

Fig. 8. (Colour online) Geochemical classification diagrams for the upper Carboniferous volcanic rocks of the Bogda-Harlik Belt (Zhao *et al.* 2014; Xie *et al.* 2016*c*; Wang *et al.* 2017; Wali *et al.* 2018): (a) Zr/TiO_2 versus Nb/Y diagram (Winchester & Floyd, 1976); and (b) Th–Zr/117–Nb/16 diagrams (Wood, 1980).

analyses (unpublished data), which is consistent with those of Lower Daheyan intrusions. The Tonggou deposit and the Lower Daheyan intrusions (303 Ma) are therefore both related to late Carboniferous magmatism.

5.d. Tectonic setting of the Bogda Mountains

In recent years, many studies have been conducted on the Bogda Mountains (Xie *et al.* 2016*a*, *b*, *c*; Wali *et al.* 2018) since it is a key area for understanding the Palaeozoic geodynamic evolution of the CAOB. There are different interpretations for the tectonic setting of the Bogda Mountains during Carboniferous time. Gu *et al.* (2000, 2001), suggested an intracontinental rift environment based on bimodal volcanism, while Shu *et al.* (2005, 2011), believed that the Carboniferous volcanic arc was superimposed by the early Permian rift with bimodal volcanism and an olistostrome. In addition, Xie *et al.* (2016*a*, *b*, *c*) suggest an island-arc setting based on the presence of high-Al basaltic lava, while Wali *et al.* (2018) support the theory of intra-arc extension based on their research on Carboniferous and lower Permian volcanic and sedimentary sequences of the Daheyan section. Previous studies mostly focus on the volcanic rocks in the Bogda Mountains, but relevant investigations on intrusions from the Bogda Mountains are limited. In this study, we present new geochronological and geochemical data for the intrusions from the southwestern part of the Bogda Mountains, and synthesize the available data for the Carboniferous magmatic rocks of the entire Bogda Mountains. The Daheyan syenogranite and coeval Sujishan granite in this belt both correspond to A-type granite (Lei *et al.* 2016*a*). A-type granites can be generated in diverse tectonic settings; however, the majority of A-type granites are affected by extension settings and are often associated with the generation of other rock types (e.g. I-type granites Wu *et al.* 2002, 2007; Ma *et al.* 2019). This is the case for the Permian stratigraphy of NE China, where A- and I-type rocks along the middle segment of the Hegenshan-Heihe Suture within the middle Great Xing'an Range were formed in a post-collisional extension setting (Ma *et al.* 2019), indicating that Daheyan A- and I-type rocks may form in a post-collisional extension setting.

In addition, the tectonic setting of late Carboniferous intrusions in the Bogda Mountains can be made clearer by the following facts. First, late Carboniferous volcanic rocks of the Bogda-Harlik Orogenic Belt clearly show a linear distribution from basalt and andesite to dacite and rhyolite on the Zr/TiO_2 versus Nb/Y diagram (Winchester & Floyd, 1976; Fig. 8a), which indicates that these rocks correspond to the calc-alkaline series. Moreover, high-Al basaltic lava and I-type intrusions are well developed in the Bogda Mountains, indicating that this magmatism formed in an arc setting (Xie *et al.* 2016*b*; this study). Second, most upper Carboniferous volcanic rocks consistently plot in the field of volcanic arcs (Fig. 8b), indicating that the upper Carboniferous volcanic rocks of the Bogda-Harlik Orogenic Belt show arc-type features and formed in a subduction zone (Chen *et al.* 2013; Xie *et al.* 2016*a*, *b*, *c*). Third, Proterozoic zircon xenocrysts in the Carboniferous and lower Permian magmatic rocks generally show positive $\epsilon_{Hf}(t)$ values (Wali *et al.* 2018; this study), suggesting the possible existence of Proterozoic juvenile crustal rocks in the basement of the Bogda Mountains and significant continental crustal growth during Carboniferous–Permian time (Kröner *et al.* 2014; Wali *et al.* 2018). As mentioned above, despite widespread changes in depositional environment from Carboniferous marine or shallow-marine environments to middle Permian terrigenous sedimentation (BGMRXUAR, 1993; Wali *et al.* 2018), a localized narrow deep-water basin appeared in a regionally shallow-marine environment during early Permian time (Shu *et al.* 2011). Based on these results, we consider that the Bogda-Harlik Orogenic Belt was still in an intra-arc extension related to a continent-based arc setting during late Carboniferous time. The Late Carboniferous Daheyan intrusions and Cu multi-metal mineralization in the Bogda Mountains therefore potentially formed in a continent-based arc setting.

6. Conclusions

(1) Late Carboniferous magmatism is intensive in the Daheyan region; rock types mainly include syenogranite, diorite, granodiorite and monzonite and ages are in the range 303–311 Ma.

https://doi.org/10.1017/S001675681900075X Published online by Cambridge University Press

(2) Syenogranite from Daheyan is an A-type granite, mainly derived from the melting of juvenile crust. Diorite from Daheyan is derived from young crust and some mixed mantle materials. Granodiorite and monzonite are both I-type granites, and sourced from the melting of juvenile crust.
(3) A comprehensive analysis of geochronological, geochemical and isotopic data of late Carboniferous magmatic rocks from the entire Bogda-Harlik Orogenic Belt suggest an intra-arc extension related to a continent-based arc setting.

Acknowledgements. We thank Editor Chad Deering and two anonymous reviewers for their constructive comments that led to the significant improvement of the manuscript. We are most grateful to the staff of the Yanduzhongshi geological analysis laboratories Ltd for LA-ICP-MS zircon U–Pb dating and Hf isotope analysis. We also thank the staff of the ALS Laboratory Group for geochemical analyses. This research was supported by the Natural Science Foundation of Xinjiang Province (grant no. 2018D01C042).

References

Allen MB, Sengor AMC and Natal'in BA (1995) Junggar, Turfan and Alakol basins as Late Permian to Early Triassic extensional structures in a sinistral shear zone in the Altaid orogenic collage, Central Asia. *Journal of the Geological Society of London* **152**, 327–38.

Allen MB, Windley BF and Zhang C (1993) Paleozoic collisional tectonics and magmatism of the Chinese Tien Shan, central Asia. *Tectonophysics* **220**, 89–115.

BGMRXUAR (Bureau of Geology and Mineral Resources of Xinjiang Uygur Autonomous Region) (1993) *Regional Geology of Xinjiang Autonomous Region, Geological Memoirs, no. 32, Map Scale* 1:500000. Beijing: Geological Publishing House (in Chinese).

Boynton WV (1984) Geochemistry of the Rare Earth Elements: Meteorite Studies. In: *Rare Earth Element Geochemistry* (ed. P Henderson), pp. 63–114. Elsevier.

Carroll AR, Graham SA, Hendrix MS, Ying D and Zhou D (1995) Late Paleozoic tectonic amalgamation of northwestern China: sedimentary record of the northern Tarim, northwestern Turpan, and southern Junggar basins. *Geological Society of America Bulletin* **107**, 571–94.

Carroll AR, Liang Y, Graham SA, Xiao X, Hendrix MS, Chu J and Mcknight CL (1990) Junggar basin, northwest China: trapped Late Paleozoic ocean. *Tectonophysics* **181**, 1–14.

Chappell BW and White AJR (1992) I- and S-type granites in the Lachlan Fold Belt. *Transactions of the Royal Society of Edinburgh Earth Sciences* **83**, 1–26.

Chen DC, Zhao XM and Deng J (2010) U-Pb dating of Carboniferous sandstone detrital zircon from the north of the Bogda Mountains, eastern Xinjiang, and its geological significances. *Acta Geologica Sinica* **84**, 1770–80.

Chen JF, Guo XS, Tang JF and Zhou TX (1999) Nd isotopic model ages: implications of the growth of the continental crust of southeastern China. *Journal of Nanjing University (Nature Science)* **35**, 649–58 (in Chinese with English abstract).

Chen X, Shu L, Santosh M and Zhao X (2013) Island arc-type bimodal magmatism in the eastern Tianshan Belt, Northwest China: Geochemistry, zircon U–Pb geochronology and implications for the Paleozoic crustal evolution in Central Asia. *Lithos* **168–169**, 48–66.

Eby GN (1990) The A-type granitoids: a review of their occurrence and chemical characteristics and speculations on their petrogenesis. *Lithos* **26**, 115–34.

Eby GN (1992) Chemical subdivision of the A-type granitoids: petrogenetic and tectonic implications. *Geology* **20**, 641–44.

Gu LX, Hu SX, Yu CS, Li HY, Xiao XJ and Yan ZF (2000) Carboniferous volcanites in the Bogda Mountains of eastern Tianshan: their tectonic implications. *Acta Petrologica Sinica* **16**, 305–16 (in Chinese with English abstract).

Gu LX, Hu SX, Yu CS, Zhao M, Wu CZ and Li HY (2001) Intrusive activities during compression–extension tectonic conversion in the Bogda intracontinental orogen. *Acta Petrologica Sinica* **17**, 187–98 (in Chinese with English abstract).

Han BF, Guo ZJ, Zhang ZC, Zhang L, Chen JF and Song B (2010) Age, geochemistry, and tectonic implications of a Late Paleozoic stitching pluton in the North Tian Shan suture zone, Western China. *Geological Society of America Bulletin* **122**, 627–40.

Hoskin PWO and Black LP (2000) Metamorphic zircon formation by solid-state recrystallization of protolith igneous zircon. *Journal of Metamorphic Geology* **18**, 423–39.

Jahn BM, Wu FY and Chen B (2000) Granitoids of the Central Asian Orogenic Belt and continental growth in the Phanerozoic. *Transactions of the Royal Society of Edinburgh Earth Sciences* **91**, 181–93.

Jung S, Hoernes S and Mezger K (2002) Synorogenic melting of mafic lower crust: constraints from geochronology, petrology and Sr, Nd, Pb and O isotope geochemistry of quartz diorites (Damara orogen, Namibia). *Contributions to Mineralogy and Petrology* **143**, 551–66.

Kröner A, Kovach V, Belousova E, Hegner E, Armstrong R, Dolgopolova A, Seltmann R, Alexeiev DV, Hoffmann JE, Wong J, Sun M, Cai K, Wang T, Tong Y, Wilde SA, Degtyarev KE and Rytsk E (2014) Reassessment of continental growth during the accretionary history of the Central Asian Orogenic Belt. *Gondwana Research* **25**, 103–25.

Lei W, Guo JF, Ma J, Xiao L, Li XC, Liu J and Li Y (2016a) Lithogeochemistry and LA-ICP-MS zircon U-Pb age and its tectonic significance of Sujishan A-type granite pluton, eastern Bogda Mountains. *Geological Journal of China Universities* **22**, 231–41 (in Chinese with English abstract).

Li P, Liu W, Zhu ZX, Chen C, Jin L, Xu S and Chen B (2013) Geochemical characteristics, geochronology and its geological significance of quartz diorite in Sangeshan area, west of Bogda, Xinjiang. *Xinjiang Geology* **31**, 162–66 (in Chinese with English abstract).

Liang T, Guo XC, Gao JG, Fan TB, Qin H, Zhou RH and Huan H (2011) Geochemistry and structure characteristic of carboniferous volcanic rocks in the eastern of Bogeda mountain. *Xinjiang Geology* **29**, 289–95 (in Chinese with English abstract).

Liu YS, Hu ZC, Gao S, Günther D, Xu J, Gao CG and Chen H (2008) In situ analysis of major and trace elements of anhydrous minerals by LA-ICP-MS without applying an internal standard. *Chemical Geology* **257**, 34–43.

Liu YS, Hu ZC, Zong KQ, Gao CG and Shan G (2010) Reappraisement and refinement of zircon U-Pb isotope and trace element analyses by LA-ICP-MS. *Science Bulletin* **55**, 1535–46.

Ludwig KR (2003) *ISOPLOT 3.0: A Geochronological Toolkit for Microsoft Excel*. Berkeley, California: Berkeley Geochronology Center, Special Publication, 1–70 pp.

Ma YF, Liu YJ, Wang Y, Tan Z, Qian C, Qin T, Feng ZQ, Sun W and Zang YQ (2019) Geochronology and geochemistry of the Carboniferous felsic rocks in the central Great Xing'an Range, NE China: Implications for the amalgamation history of Xing'an and Songliao-Xilinhot blocks. *Geological Journal* **54**, 482–513.

Maniar PD and Piccoli PM (1989) Tectonic discrimination of granitoids. *Geological Society of American Bulletin* **101**, 635–43.

Middlemost EAK (1994) Naming materials in the magma/igneous rock system. *Earth Science Reviews* **37**, 215–24.

Patiño Douce AE and Johnston AD (1991) Phase equilibria and melt productivity in the pelitic system: implications for the origin of peraluminous granitoids and aluminous granulites. *Contributions to Mineralogy and Petrology* **107**, 202–18.

Peccerillo A and Taylor AR (1976) Geochemistry of Eocene calc-alkaline volcanic rocks from the Kastamonu area, Northern Turkey. *Contributions to Mineralogy and Petrology* **58**, 63–81.

Pirajno F, Mao JW, Zhang ZC, Zhang ZH and Chai FM (2008) The association of mafic–ultramafic intrusions and A-type magmatism in the Tianshan and Altay orogens, NW China: implications for geodynamic evolution and potential for the discovery of new ore deposits. *Journal of Asian Earth Sciences* **32**, 165–83.

Qin KZ, Su BX, Sakyi PA, Tang DM, Li XH, Sun H, Xiao QH and Liu PP (2011) SIMS zircon U–Pb geochronology and Sr–Nd isotopes of Ni–Cu-bearing mafic–ultramafic intrusions in Eastern Tianshan and Beishan in correlation with flood basalts in Tarim Basin (NW China): constraints on a ca. 280 Ma mantle plume. *American Journal of Science* **311**, 237–60.

Rapp RP and Watson EB (1995) Dehydration melting of metabasalt at 8-32 kbar: implications for continental growth and crust-mantle recycling. *Journal of Petrology* **36**, 891–931.

https://doi.org/10.1017/S001675681900075X Published online by Cambridge University Press

Searle MP, Parrish RR, Hodges KV, Hurford A, Ayres MW and Whitehouse MJ (1997) Shisha Pangma Leucogranite, South Tibetan Himalaya: field relations, geochemistry, age, origin, and emplacement. *Journal of Geology* **105**, 295–318.

Shu L, Wang B, Zhu W, Guo Z, Charvet J and Zhang Y (2011) Timing of initiation of extension in the Tianshan, based on structural, geochemical and geochronological analyses of bimodal volcanism and olistostrome in the Bogda Shan (NW China). *International Journal of Earth Sciences* **100**, 1647–63.

Shu LS, Zhu WB, Wang B, Faure M, Charvet J and Cluzel D (2005) The post-collision intracontinental rifting and olistostrome on the southern slope of Bogda Mountains, Xinjiang. *Acta Petrologica Sinica* **21**, 25–36 (in Chinese with English abstract).

Si G, Su H, Yang G, Zhang C and Yang G (2014) Geological significance and geochemical characteristics of the Sikeshu pluton in north Tianshan, Xinjiang. *Xinjiang Geology* **32**, 19–24 (in Chinese with English abstract).

Su BX, Qin KZ, Sun H, Tang DM, Sakyi PA, Chu ZY and Xiao QH (2012) Subduction-induced mantle heterogeneity beneath Eastern Tianshan and Beishan: Insights from Nd–Sr–Hf–O isotopic mapping of Late Paleozoic mafic–ultramafic complexes. *Lithos* **134–135**, 41–51.

Sun G, Li J, Gao L and Yang T (2005) Zircon SHRIMP U–Pb age of a dioritic pluton in the Harlik Mountain, Eastern Xinjiang, and its tectonic implication. *Geological Review* **51**, 463–69 (in Chinese with English abstract).

Sun SS and McDonough WF (1989) Chemical and isotopic systematics of oceanic basalts: implications for mantle composition and processes. In: *Magmatism In Ocean Basins* (eds AD Saunders and MJ Norry), pp. 313–45. Geological Society of London, Special Publication no. 42.

Wali G, Wang B, Cluzel D and Zhong L (2018) Carboniferous-Early Permian magmatic evolution of the Bogda Range (Xinjiang, NW China): Implications for the Late Paleozoic accretionary tectonics of the SW Central Asian Orogenic Belt. *Journal of Asian Earth Sciences* **153**, 238–51.

Wang B, Shu L, Faure M, Jahn BM, Cluzel D, Charvet J, Chung Sl and Meffre S (2011) Paleozoic tectonics of the southern Chinese Tianshan: insights from structural, chronological and geochemical studies of the Heiyingshan ophiolitic mélange (NW China). *Tectonophysics* **497**, 85–104.

Wang C, Chen B, Ma XH and Yan XL (2015) Petrogenesis of early and late Paleozoic plutons in Sanchakou area of east Tianshan and their implications for evolution of Kangur Suture Zone. *Journal of Earth Sciences Environment* **37**, 52–70 (in Chinese with English abstract).

Wang C, Ma XH, Chen B and Yan XL (2017) Late Carboniferous volcanism of the Harlik orogenic belt, Xinjiang: Zircon U-Pb geochronological, geochemical and Sr-Nd isotopic evidence. *Acta Petrologica Sinica* **33**, 440–54 (in Chinese with English abstract).

Watson EB and Harrison TM (1983) Zircon saturation revisited: temperature and composition effects in a variety of crustal magma types. *Earth and Planetary Science Letters* **64**, 295–304.

Whalen JB, Currie KL and Chappell BW (1987) A-Type granites: geochemical characteristics, discrimination and petrogenesis. *Contributions to Mineralogy and Petrology* **95**, 407–19.

Winchester JA and Floyd PA (1976) Geochemical magma type discrimination: application to altered and metamorphosed basic igneous rocks. *Earth and Planetary Science Letters* **28**, 459–69.

Wood DA (1980) The application of a Th–Hf–Ta diagram to problems of tectonomagmatic classification and to establishing the nature of crustal contamination of basaltic lavas of the British tertiary volcanic province. *Earth & Planetary Science Letters* **50**, 11–30.

Wu FY, Sun DY, Li HM, Jahn BM and Wilde SA (2002) A-type granites in northeastern China: age and geochemical constraints on their petrogenesis. *Chemical Geology* **187**, 143–73.

Wu FY, Zhao GC, Sun DY, Wilde SA and Yang JH (2007) The Hulan Group: Its role in the evolution of the Central Asian Orogenic Belt of NE China. *Journal of Asian Earth Sciences* **30**, 542–56.

Wu YS, Chen YJ and Zhou KF (2016) Mo deposits in Northwest China: Geology, geochemistry, geochronology and tectonic setting. *Ore Geology Reviews* **81**, 641–71.

XBGMR (Xinjiang Bureau of Geology and Mineral Resources) (1988) Geological Map 1:200000, Dabancheng-Tuokexun Sheet (L-45-5 and L-45-11).

Xia LQ, Xia ZC, Xu XY, Li XM, Ma ZP and Wang LS (2004) Carboniferous Tianshan igneous megaprovince and mantle plume. *Geological Bulletin of China* **23**, 903–10 (in Chinese with English abstract).

Xiao B, Chen H, Hollings P, Han JS, Wang YF, Yang JT and Cai KD (2017) Magmatic evolution of the Tuwu-Yandong porphyry Cu belt, NW China: constraints from geochronology, geochemistry and Sr-Nd-Hf isotopes. *Gondwana Research* **43**, 74–91.

Xiao WJ, Windley BF, Allen MB and Han C (2013) Paleozoic multiple accretionary and collisional tectonics of the Chinese Tianshan orogenic collage. *Gondwana Research* **23**, 1316–41.

Xiao WJ, Zhang LC, Qin KZ, Sun S and Li JL (2004) Paleozoic accretionary and collisional tectonics of the eastern Tianshan (China): implications for the continental growth of Central Asia. *American Journal of Science* **304**, 370–95.

Xie W, Luo ZY, Xu YG, Chen YB, Hong LB, Ma L and Ma Q (2016a). Petrogenesis and geochemistry of the Late Carboniferous rear-arc (or back-arc) pillow basaltic lava in the Bogda Mountains, Chinese North Tianshan. *Lithos* **244**, 30–42.

Xie W, Xu YG, Chen YB, Luo ZY, Hong LB, Ma L and Liu HQ (2016b) High-alumina basalts from the Bogda Mountains suggest an arc setting for Chinese Northern Tianshan during the Late Carboniferous. *Lithos* **256–257**, 165–81.

Xie W, Xu YG, Luo ZY, Liu HQ, Hong LB and Ma L (2016c) Petrogenesis and geodynamic implications of the Late Carboniferous felsic volcanics in the Bogda belt, Chinese Northern Tianshan. *Gondwana Research* **39**, 165–79.

Xu B, Charvet J, Chen Y, Zhao P and Shi G (2012) Middle Paleozoic convergent orogenic belts in western Inner Mongolia (China): framework, kinematics, geochronology and implications for tectonic evolution of the Central Asian Orogenic Belt. *Gondwana Research* **23**, 1342–64.

Yakubchuk A (2017) Evolution of the Central Asian Orogenic Supercollage since Late Neoproterozoic revised again. *Gondwana Research* **2017**, 47.

Yuan C, Sun M, Wilde S, Xiao W, Xu Y, Long X and Zhao G (2010) Post-collisional plutons in the Balikun area, East Chinese Tianshan: Evolving magmatism in response to extension and slab break-off. *Lithos* **119**, 269–88.

Zhang HF, Parrish R, Zhang L, Xu WC, Yuan HL, Gao S and Crowley QG (2007) A-type granite and adakitic magmatism association in Songpan–Garze fold belt, eastern Tibetan Plateau: Implication for lithospheric delamination. *Lithos* **97**, 323–35.

Zhang HX, Niu HC, Terada K, Yu XY, Sato H and Ito J (2003) Zircon SHRIMP U-Pb dating on plagiogranite from Kuerti ophiolite in Altay, North Xinjiang. *Chinese Science Bulletin* **48**, 2231–2235 (in Chinese with English abstract).

Zhao TY, Xu SQ, Zhu ZX, Liu X and Chen C (2014) Geological and geochemical features of carboniferous volcanic rocks in Bogda-Harlik Mountains, Xinjiang and their tectonic significance. *Geological Review* **60**, 115–24 (in Chinese with English abstract).

https://doi.org/10.1017/S001675681900075X Published online by Cambridge University Press